A conserved Hsp70 phosphorylation regulates cell cycle progression after DNA damage

Thomas Moss[1,2], Alexandra Wooldredge[1,2], Koustav Bhakta[1,2], Matthew Cronin[1,2], Jason E. Gestwicki[3], Shaeri Mukherjee[1,2,4#]

[1]G.W. Hooper foundation, University of California at San Francisco, San Francisco, USA.

[2]Department of Microbiology and Immunology, University of California at San Francisco, San Francisco, USA.

[3]Department of Pharmaceutical Chemistry and the Institute for Neurodegenerative Diseases, University of California San Francisco, San Francisco, CA, USA

[4]Chan Zuckerberg Biohub, San Francisco, USA.

[#] - Corresponding author: shaeri.mukherjee@ucsf.edu

ABSTRACT

Hsp70s are essential molecular chaperones that are increasingly recognized to be regulated by post-translational modifications. Here, we show that phosphorylation of a conserved threonine (T495), previously shown to be exploited by a *Legionella pneumophila* kinase to inhibit Hsp70, occurs endogenously in human cells in response to DNA damage, particularly when base excision repair is overburdened. This modification is cell cycle dependent, and in yeast, phosphomimetic or phosphonull Hsp70 variants disrupt G1/S progression under normal and DNA-damaging conditions. Biochemically, the phosphomimetic T495E mutation locks Hsp70 in an open-like conformation without blocking substrate engagement. Together, our results reveal a conserved mechanism by which dynamic Hsp70 phosphorylation regulates the G1/S transition, and delays cell cycle progression during DNA damage, highlighting how pathogen-derived insights can uncover fundamental cell biology principles.

INTRODUCTION

Hsp70s are highly conserved molecular chaperones with wide-ranging roles in cellular homeostasis. At the core of their function is an ATP-driven conformational cycle: Hsp70s alternate between an open ATP-bound state and a closed ADP-bound state, enabling them to bind and release client proteins in a nucleotide-dependent manner[1]. Through this mechanism, Hsp70s participate in diverse biological processes, including protein homeostasis[1], metabolic regulation[2], the DNA damage response[3], and cell cycle control[4,5]. Beyond their central roles in cell biology Hsp70s have been implicated in the pathology of numerous diseases. For example, Hsp70s can inhibit amyloid-beta aggregation *in vitro* and reduce its accumulation in mouse neurons, suggesting protective roles in neurodegenerative diseases such as Alzheimer's disease[6,7]. Hsp70s are also overexpressed in various cancers and influence tumor cell survival and proliferation [8]. Thus, understanding how Hsp70 activity is regulated has broad implications for both basic biology and therapeutic development.

Hsp70 function is tightly controlled by co-chaperones and post-translational modifications (PTMs). Cochaperones — namely J proteins and nucleotide exchange factors — catalyze nucleotide hydrolysis and exchange, facilitate and specify client engagement, and determine client fate [1]. In recent years, PTMs have emerged as an important layer of regulation. A computational analysis of the budding yeast Hsp70, Ssa1, identified two conserved 'hotspots' in the nucleotide binding domain (NBD) and substrate binding domain (SBD), that are likely regions of PTM-mediated regulation[9]. Experimental work has validated some of the PTMs at these site. For example, T36 in the NBD of Ssa1 is phosphorylated both in response to nutrient stress and exposure to mating pheromone (α-factor), impairing chaperone activity and leading to cell cycle arrest[4]. In mammalian cells, the endoplasmic reticulum (ER) resident Hsp70, BiP, is AMPylated at T518, locking it in an 'open' conformation and tuning its activity to the unfolded protein burden in the ER [10,11]. Our lab previously showed that the *Legionella pnuemophila* (*L.p.*) kinase LegK4 phosphorylates cytosolic human Hsp70 (Hsc70; HSPA8) at T495 during infection, increasing its association with polysomes and globally reducing protein synthesis[12]. Notably, Hsc70(T495) is structurally analogous to BiP(T518), indicating that both AMPylation and phosphorylation at this site have regulatory consequences. This finding led us to ask whether phosphorylation at T495 occurs outside of *L.p.* infection, and if it serves endogenous regulatory functions. Mining phosphoproteomics datasets revealed that the homologous residue in *S. cerevisiae* Ssa1, T492, is phosphorylated during DNA alkylation damage, and when mitotic exit is prevented[13,14]. However, the functional consequences of this modification have not been studied. In this work, we show that Hsp70 is phosphorylated at T495 (pHsp70) in human cells during base excision repair (BER) of DNA damage. We find that a phosphomimetic mutant T495E allosterically impairs ATP hydrolysis *in vitro* and stabilizes an open-like conformation while still permitting substrate engagement. In yeast, the analogous mutation T492E causes a growth defect, leads to accumulation of cells in G1, and delays cell

cycle re-entry after alkylation damage. Likewise, the phosphonull mutation (T492A) in yeast lacking a compensatory Hsp70 homolog also causes a growth defect and cell cycle dysregulation after alkylation damage. Together, these data suggest that the dynamic phosphorylation of Hsp70 at this conserved site acts as a regulatory switch to tune chaperone activity in coordination with DNA repair and cell cycle progression.

RESULTS

Phosphomimetic Hsc70 (T495E) is locked in an open-like conformation

Previous work showed that the *Legionella pneumophila* kinase LegK4 phosphorylates Hsc70 at a conserved threonine (T495) in its substrate SBD (Figure 1a), reducing its chaperone activity[12]. However, *in vitro* phosphorylation by LegK4 only yields phosphorylation of ~53% of the Hsc70, complicating bulk biochemical analyses [12]. To overcome this limitation, we generated a phosphomimetic mutant Hsc70 (T495E). To determine whether this mutant mimics phosphorylated Hsc70, we assessed the ATPase activity of the purified protein using a malachite green assay. As Hsc70 has a low intrinsic rate of ATPase activity, we titrated in the co-chaperone DnaJA2 to stimulate hydrolysis[12,15]. T495E exhibited significantly reduced J-protein stimulated ATPase activity compared to wild-type Hsc70 (WT) (Figure 1b), consistent with prior observations of the LegK4-phosphorylated protein[12]. To investigate if the reduced ATPase activity is due to impaired nucleotide binding, we performed a fluorescence polarization (FP) assay using fluorescently-labeled ATP-FAM. ATP binding was not diminished in T495E (Figure 1c), suggesting that T495E allosterically inhibits J protein stimulated ATPase activity without preventing nucleotide binding.

Hsp70 chaperone activity is driven by cycling through nucleotide-dependent conformations[1]. In the ATP-bound state, Hsp70s adopt an ‘open’ conformation, and ATP hydrolysis to ADP induces large-scale structural rearrangements to a ‘closed’ state[1]. As T495E poorly hydrolyzes ATP, we reasoned that this mutation may lock the protein into either the open or closed conformation. Indeed, AMPylation of BiP at the analogous residue is known to lock the protein in an open state[16]. To assess the conformation of T495E Hsc70, we performed partial proteolysis using trypsin, which produces distinct cleavage patterns depending on the protein’s conformation[17,18]. As expected, WT Hsc70 displayed nucleotide-dependent banding: protection of band 2 and loss of band 3 in the presence of ADP compared to ATP. In contrast, T495E exhibited an ATP-like banding pattern regardless of nucleotide, consistent with a locked open conformation (Figure 1d). While this agrees with the studies on BiP AMPylation, our previous work showed that phosphorylation coincides with increased occupancy of Hsc70 on polysomes, suggesting continued substrate engagement[12]. We therefore asked whether T495E can still bind client proteins. An ELISA with tau, a known Hsc70 substrate[19], showed that T495E retains the ability to bind tau despite the conformational lock (Figure 1e). These results suggest that T495E locks Hsc70 in a pseudo-open conformation: structurally similar to the ATP-bound open state in terms of protease sensitivity and domain exposure, yet still capable of substrate engagement typically associated with the closed state.

Base excision repair leads to Hsp70(T495) phosphorylation

Pathogens often mimic host proteins and hijack cellular pathways to create a favorable niche for replication. Thus, these pathogen-driven modifications frequently reveal biologically significant regulatory nodes within host systems[20]. Motivated by this concept, we asked whether the phosphoregulation of Hsp70 employed by *Legionella* might occur endogenously in mammalian cells. A phospho-proteomics study in *S. cerevisiae* identified phosphorylation at the analogous residue, Ssa1(T492), after treatment with the alkylating agent methyl

methanesulfonate (MMS)[13]. Inspired by this finding, we analyzed human cells treated with MMS and observed that this phosphorylation is conserved(Figure 2a).

This finding suggested that phosphorylation of Hsp70 might be involved in the response to DNA damage. MMS is primarily used as a DNA alkylating agent, though its chemical activity is not limited to DNA targets[21]. Thus, we sought to determine whether the response to MMS-induced DNA alkylation leads to Hsp70 phosphorylation. Aberrant DNA alkylation is predominantly repaired through the base excision repair (BER) pathway[22]. In BER, DNA glycosylases recognize and excise damaged bases, producing an abasic site (AP site). MMS-induced lesions are processed by N-methylpurine DNA glycosylase (MPG)[22,23] (Figure 2b). The backbone at the AP site is then cleaved by the endonuclease APE1, and the resultant single stranded break is repaired by a variety of proteins, including the DNA polymerase Polβ[22] (Figure 2b). Interestingly, the predominant DNA adduct generated by MMS, 7-methylguanine, is not intrinsically cytotoxic, but spontaneously depurinates to a toxic and mutagenic intermediate and so requires rapid repair[24,25]. The repair intermediates generated by the BER pathway, however, are cytotoxic[24]. Because Polβ activity is rate limiting, overexpression of the glycosylase that initiates BER can lead to an accumulation of these cytotoxic intermediates[22,26]. To determine whether increased BER activity affects Hsp70 phosphorylation, we treated cells overexpressing MPG with MMS. MPG overexpression modestly increased MMS-induced pHsp70 levels (Figure 2c). Conversely, inhibition of the subsequent BER step strongly reduced the levels of MMS-induced pHsp70. Pharmacological inhibition of APE1 led to a dose dependent decrease in Hsp70 phosphorylation (Figure 2d). Similarly, treatment with methoxyamine (Mx), which covalently binds AP sites and impairs APE1 cleavage and Polβ activity[27], caused a striking reduction in pHsp70 levels (Figure 2b,e). Surprisingly, overexpression of APE1 did not enhance pHsp70 (Figure S1a), suggesting that APE1 activity is necessary but not rate-limiting in this context. Additionally, overexpression of Polβ did not reduce pHsp70 upon MMS treatment (Figure S1b).These data confirm that the DNA alkylation by MMS is responsible for Hsp70 phosphorylation in human cells, and the results specifically indicate that BER intermediates may trigger this response.

To test the specificity of Hsp70 phosphorylation in response to DNA damage, we treated cells with a panel of genotoxic compounds that activate distinct branches of the DNA damage response (DDR), including bleomycin (induces double stranded breaks), camptothecin (a topoisomerase I inhibitor), hydroxyurea (depletes the dNTP pool), MMS, and arsenite (generates reactive oxygen species). While activation of DDR kinases (pDNA-PKcs(S2056), pATM(S1981) pChk2(T68), pChk2(S516)), and an increase of the DDR marker γH2AX confirm DNA damage and response induction in the drug treatment conditions, pHsp70 was only observed following high-dose MMS treatment, and exposure to sodium arsenite (Figure 2f). Arsenite causes oxidative DNA damage that can be repaired through BER[22,28]. Surprisingly, arsenite has also been shown to both inhibit the activity of enzymes necessary for this pathway, including OGG (the oxidative glycosylase)[29], and decrease the levels of others (e.g. APE1 and Polβ) [30]. Despite this, we found that both treatment with Mx and inhibition of APE1 were still sufficient to prevent Hsp70 phosphorylation upon arsenite treatment (Figure S1c,d). These findings suggest that Hsp70(T495) phosphorylation is selectively triggered by repair intermediates generated during BER.

Phosphorylation of Hsp70 requires the DDR kinases ATM, DNA-PKcs, Chk2, and CK1

Though BER can function as a self-contained repair pathway, several DDR kinases are known to facilitate its activity[31,32]. To determine if DDR signaling contributes to MMS-induced Hsp70 phosphorylation, we performed siRNA-mediated knockdowns of the three master kinases of the DDR: ataxia-telangiectasia mutated (ATM), ataxia-telangiectasia and Rad3-related (ATR), and DNA-dependent protein kinase catalytic subunit (DNA-PKcs). Among these, only knockdown of DNA-PKcs prevented Hsp70 phosphorylation (Figure 3a, Supp Figure 2a,b). Interestingly, while ATM knockdown had no effect, pharmacological inhibition of ATM decreased Hsp70

phosphorylation (Figure 3b). To rule out off-target effects, we tested two independent ATM inhibitors and observed a similar reduction in pHsp70 with both (Figure 3b). This discrepancy is consistent with prior reports showing that genetic and pharmacological inhibition of ATM can yield diverging results[33,34]. Pharmacological inhibition of DNA-PKcs confirmed the DNA-PKcs knockdown experiment (Figure 3c). Both DNA-PKcs and ATM phosphorylate the transducer kinase Chk2, activating it and promoting propagation of the DDR[35]. Inhibition of Chk2 also prevented Hsp70 phosphorylation (Figure 3c). Given that casein kinase 1 (CK1) has been previously reported to act in concert with Chk2 in the DDR[36], we tested its involvement and found that CK1 inhibition also suppressed Hsp70 phosphorylation (Figure 3d, Figure S2c). Inhibition of these kinases also prevented Hsp70 phosphorylation upon arsenite treatment (Figure S2d).

Having identified a set of kinases required for Hsp70 phosphorylation, we noted that the delayed timing of this event is striking. Canonical DDR signaling is initiated within minutes of damage induction[31,37], yet pHsp70 only emerges after prolonged MMS exposure (Fig 3d). Indeed, we observed robust activation of DNA-PKcs, ATM and Chk2 well before Hsp70 phosphorylation (Figure 3d). These observations raise the possibility that either prolonged MMS exposure or a secondary cellular response is required to trigger Hsp70 phosphorylation.

Hsp70 phosphorylation occurs after M phase onset

To better understand the timing of Hsp70 phosphorylation, we treated cells with MMS for varying durations (1 to 5 hours), followed by recovery in fresh media up to a total of 5 hours. In previous experiments, we observed robust Hsp70 phosphorylation only after 5 hours of continuous MMS treatment, with minimal signal at earlier timepoints (see Fig. 3d). However, in our pulse-chase assay, 2 hour MMS treatment, when followed by a 3 hour MMS-free chase, resulted in pHsp70 accumulation (Fig. 4a). This result indicates that prolonged MMS exposure alone does not fully explain the lag time between damage initiation and the appearance of pHsp70, suggesting that secondary cellular events or signaling contribute to Hsp70 phosphorylation.

Damage from MMS is thought to occur when replication forks collide with DNA repair intermediates in S phase[38]. This hypothesis, in combination with our observations that pHsp70 accumulation lags behind initial DDR activation, suggested that cell cycle stage might be a key determinant in Hsp70 phosphorylation. In asynchronous populations, Hsp70 phosphorylation might only appear when enough cells reach a permissive phase of the cell cycle. If this were true, synchronizing cells at the beginning of S phase should potentiate MMS-induced Hsp70 phosphorylation. To test this idea, we synchronized cells at the beginning of S phase using a double thymidine block, then released them into MMS-containing or untreated media. Unexpectedly, synchronization at G1/S does not increase Hsp70 phosphorylation (Figure 4b). Even more surprising, MMS-treated cells entered mitosis at an increased rate compared to controls, as evidenced by the accumulation of the mitotic marker phospho-Histone H3 (S10) (pH3), reduced levels of S phase markers such as the replication licensing factor CDT1 and thymidine kinase, and pCdk1 (Y15), the inhibited cyclin dependent kinase that must be de-phosphorylated for M phase entry (Figure 4b). These data suggest that MMS drives cells into mitosis, and that Hsp70 phosphorylation occurs after this transition. Indeed, blocking mitotic entry by treatment with a CDK1 inhibitor (Ro3306) prevented both MMS and arsenite induced Hsp70 phosphorylation (Figure 4c, Figure S3a). Releasing the CDK1 block upon MMS or arsenite treatment restored Hsp70 phosphorylation (Figure 4c, Figure S3a), suggesting this response does not require passage through S phase. While passage through mitosis upon DNA damage is necessary for Hsp70 phosphorylation, the presence of pHsp70 in a distinct nuclear fraction indicates that it persists after nuclear envelope reformation (Figure 4d). Indeed, a 2 hour pulse chase of MMS revealed that pHsp70 accumulates even after pH3 disappears, indicating that phosphorylation is maintained after mitotic exit (Figure 4e). Notably, we do not see an increase of S phase markers such as thymidine kinase, nor changes in cyclin A or cyclin B levels, suggesting that the cell cycle progression may be dysregulated following MMS treatment.

Phosphoregulation of Ssa1 at T492 is important for G1/S transition in yeast

To investigate the functional significance of Hsp70 phosphorylation at T495, we turned to *S. cerevisiae* due to its genetic tractability. *S. cerevisiae* has four cytosolic Hsp70s, Ssa1-4. Of these, Ssa1 and Ssa2 are constitutively expressed, whereas Ssa3 and Ssa4 are stress-inducible[39]. Phosphoproteomics studies revealed that Ssa1 can be phosphorylated at threonine 492, which corresponds to human Hsp70 T495[13,14]. To probe the role of this modification, we created phosphomimetic (T492E, TE) and phosphonull (T492A, TA) point mutations at the endogenous SSA1 locus. Given the known redundancy between Ssa1 and Ssa2[40], we disrupted SSA2 by inserting an antimicrobial resistance gene into its coding sequence to better assess the functional consequences of Ssa1 phospho-variants. Strikingly, even in the SSA2 background, we observed a growth defect in TE yeast (Figure 5a,b). This is not likely explained by hypomorphism, as neither the TA mutant nor the WT;*ssa2*Δ strains show such a defect. Rather, phosphomimetic Ssa1 seems to act in a dominant manner. In the *ssa2*Δ background, strains expressing either phosphomimetic or phosphonull Ssa1 grew more slowly than the wild-type (Figure 5 a,b).

Phosphorylation of Ssa1 at T492 was previously reported to occur in a cell cycle dependent manner, specifically when yeast are prevented from exiting mitosis through the expression of a non-degradable cyclin B[14]. This information, in conjunction with the cell cycle dependence of pHsp70 in human cells and the growth defects we observed in our yeast phosphomutants, led us to examine the impact of these mutations on cell cycle progression. With SSA2 present, the Ssa1 WT and phosphonull (TA) strains showed similar cell cycle distributions. In contrast, the phosphomimetic mutant (TE) showed an increase in cells with 1N DNA content, consistent with a G1 stall (Figure 5c). In the *ssa2*Δ background for both Ssa1 WT and TA, we see a slight increase in the G1 population compared to G2, and the difference is even more pronounced in T492E yeast (Figure 5c). T492A yeast showed increased cell size in G1 in the *ssa2*Δ background, a phenotype previously linked to G1/S stalling, perhaps due to decreased Cln3 stability[4] (Figure S4a). Intriguingly, both Δ*ssa2* point mutants exhibited a large cell size in G2/M (Figure S4a) — a finding that warrants additional investigation. Together, these data suggest that dynamic phospho-regulation of Ssa1 at T492 is critical for proper cell cycle progression.

We were curious if this modification served a similar cell cycle regulatory function during MMS treatment. To assess the overall viability of the point mutants in response to alkylation damage we performed a spot test in the presence and absence of MMS. In the *ssa2*Δ background, both phosphonull and phosphomimetic Ssa1 led to impaired growth on MMS-containing media, though growth in the in the SSA2 background was only mildly impacted (Figure 5d). To examine how these mutations influence cell cycle progression in response to MMS, we treated the strains with 0.05% MMS for three hours as previously shown to cause Ssa1 phosphorylation at T492[13], and released them into fresh YPAD for the indicated times (Figure 5e). Ssa1 WT strains with and without SSA2 behave similarly: immediately after the MMS treatment the cells display a bimodal distribution around G1 and early S. Upon MMS release, the G1 peak gradually disappeared, accompanied by synchronized progression through S phase, with DNA content slowly increasing over time. In the SSA2 background, the T492A was nearly indistinguishable from the WT strains. However, in the *ssa2*Δ background, T492A no longer exhibited the bimodal distribution of cells near 1N immediately after MMS treatment. Rather, there was a single peak. Upon release, the cells failed to undergo coordinated S phase progression. Instead, DNA content increased in an asynchronous manner, suggesting impaired checkpoint regulation. The T492E mutants also showed distinct phenotypes. In the SSA2 background, T492E cells lacked the bimodal distribution around 1N immediately after MMS treatment, and instead exhibited a more pronounced G1 arrest. Upon release, these cells progressed through S phase more slowly than WT, with a prominent left shoulder, indicating delayed DNA replication in a subset of cells. In the *ssa2Δ* background, the phenotype was even more prominent. A strong 1N peak persisted after MMS release, with

minimal evidence of bulk S phase progression. Instead, we observed a gradual increase in DNA content across the population, reminiscent of the T492A mutant in *ssa2Δ*, but with a key difference: while T492A;*ssa2*Δ cells showed more rapid entry to and passage through S phase, T492E;*ssa2Δ* cells retained a distinct 1N peak and slower S phase progression. These data indicate that both phosphonull and phosphomimetic mutations disrupt the coordination of cell cycle re-entry following genotoxic stress. Loss of phosphorylation appears to weaken G1 arrest and promote uncontrolled S-phase entry, while constitutive phosphorylation reinforces arrest but impairs orderly progression through S phase. Eliminating the functional redundancy of Ssa2 in the T492A;*ssa2*Δ and T492E;*ssa2*Δ strains reveals the importance of dynamic Ssa1 phospho-regulation in mounting an effective DNA damage response and ensuring proper cell cycle transitions**,** as both phosphonull and phosphomimetic Ssa1 variants result in cell cycle dysregulation and altered growth in the absence of Ssa2.

DISCUSSION

Our work demonstrates that Hsp70s are phosphorylated at T495 as part of a conserved response to DNA damage, and that dynamic phosphoregulation of this residue exerts control over the cell cycle. While prior phosphoproteomics studies in yeast detected phosphorylation of the analogous residue in Ssa1 (T492) following MMS exposure[13] or mitotic exit block[14], our findings establish that this modification is a regulated, damage-responsive event that is conserved in human cells. We show that phosphorylation is induced by two chemically distinct DNA-damaging agents, MMS and sodium arsenite, both of which generate BER substrates. Critically, inhibition of the BER endonuclease APE1 or chemical blockade of abasic site recognition and repair abolishes pHsp70 formation. Of note, high doses and long treatment times are required to elicit Hsp70 phosphorylation with both compounds, which raises questions as to the precise driver of this response. BER is a streamlined pathway: it is thought to follow a 'baton-passing' model, with each enzyme passing off intermediates to the next in the cascade[41]. However, BER intermediates are cytotoxic. APE1-mediated cleavage of the DNA backbone produces single-strand breaks that, if encountered by replication forks, can be converted into double-stranded breaks (DSBs)[38]. The requirement for APE1 activity, along with the involvement of the DSB repair kinases ATM and DNA-PKcs, support a model in which BER-induced DSBs lead to Hsp70 phosphorylation.

While it is clear that Hsp70 is phosphorylated in response to DNA damage, the lag time between insult and pHsp70 suggests a complex signaling pathway. Phosphorylation does not arise simply during damage exposure; instead, it requires both prolonged insult and progression through mitosis. Despite the longstanding view that MMS-induced damage primarily arises during S phase, we find that synchronizing cells at G1/S does not enhance Hsp70 phosphorylation. This paradox may be resolved by emerging evidence that BER-induced DSBs can occur in non-replicating cells[42]. Considering that the DDR is considerably rewired during mitosis, and though BER occurs, repair of lesions such as DSBs is forestalled until mitotic exit[43–45], it is possible that pHsp70 arises in response to high lesion burden in M phase to prevent cell cycle entry into the vulnerable S phase (Figure 6a).

Our genetic studies in yeast directly link phosphoregulation of Ssa1 at T492 to cell cycle progression. Both phosphonull (T492A) and phosphomimetic (T492E) mutants cause growth defects in the absence of the compensatory isoform Ssa2, underscoring the importance of dynamic, reversible phosphorylation at this site. Cell cycle profiling reveals that T492E yeast in both SSA2 and *ssa2*Δ backgrounds accumulate in G1 and fail to efficiently enter S phase following MMS exposure, while T492A strains show delayed recovery in the absence of Ssa2. Further, in the absence of MMS insult, the Ssa1 T492E mutant strain exhibits altered growth and cell cycle progression even in the SSA2 background, suggesting a dominant effect of the phosphomimetic variant. The dominant phenotype of T492E is consistent with biochemical data suggesting persistent, aberrant substrate engagement, akin to the effects of mutations that trap Hsp70 in a

closed conformation[46]. Together, these results support a model in which pHsp70 serves as a reversible molecular brake, preventing premature S-phase entry under conditions of BER stress.

Interestingly, this mechanism parallels, but is distinct from the previously described phospho-Ssa1 (T36) mediated regulation of the cell cycle. Phosphorylation at T36/38 also enforces G1/S arrest in yeast. However, the residue is in the NBD, and phosphorylation decreases nucleotide binding. Furthermore, the activity is ER-localized, where it slows the accumulation of Cdk1-Cln3 by sequestering and promoting the degradation of Cln3[4]. In contrast, pT492/495 occurs in the SBD, modulates ATP hydrolysis without preventing nucleotide binding, and occurs in the nucleus. Given the established role of phosphorylation in directing Hsp70-client fate [47,48], it is plausible that pT492/T495 controls the stability or activity of nuclear substrates critical for G1/S transition. Our data support a model wherein Hsp70 engagement with both a client and some accessory machinery (e.g. a cochaperone) are controlled by phosphorylation to regulate S phase entry (Figure 6b). For instance, if a specific Hsp70 client must be degraded to exit G1, phosphorylation may promote engagement with said client and proper degradation machinery, and dephosphorylation could allow client release. In this case, the phosphomimetic Hsp70 would be unable to disengage, and therefore cause the G1/S stall we report. Conversely, the phosphonull Hsp70 would be unable to establish proper interactions with the client and/or accessory machinery, thereby preventing efficient degradation and leading to the observed dysregulation of S phase re-entry. While this model explains our experimental observations, other possibilities remain, and future work is required to further establish mechanistic details.

Collectively, our findings reveal a conserved phospho-switch on Hsp70 that links DNA damage sensing during BER to cell cycle control, adding an unanticipated regulatory layer to the integration of repair and checkpoint pathways. Strikingly, this pathway came to light because it is targeted by a pathogenic effector kinase, once again illustrating how pathogens can hijack, and thereby illuminate, fundamental aspects of cell biology. Such examples underscore the enduring value of pathogens as powerful tools to uncover deeply conserved regulatory mechanisms. This work opens the door to identifying the upstream kinase(s) and downstream client(s) that mediate this effect, and to determining whether T495 phosphorylation serves as a general mechanism for coordinating repair with proliferation in diverse physiological contexts. By coupling BER to a reversible molecular brake on S phase entry, phosphorylation of Hsp70 at T495 emerges as a conserved checkpoint signal that safeguards genome integrity under conditions of repair-induced stress.

RESOURCES

Plasmids

Description	ID	Source
Hsc70 in pMCSG7	pSM226	Moss 2019[12]
Hsc70(T495E) in pMCSG7	pSM227	Moss 2019[12]
LegK4Δ1-58 in pEGFP-C2	pSM160	Moss 2019[12]
MPG in pIRESNeo	pSM282	Addgene Plasmid #12548
APE1 in pCMVd3	pSM303	This study
pCMVd3 empty vector	pSM304	This study
Polβ in pLVX-GWE-IRES-puro	pSM288	Addgene Plasmid #128653
plVX-GWE-IRES-puro empty vector	pSM289	This study
pYM13 PCR template KanMX resistance	pSM302	Gift from David O. Morgan Lab

RNA Oligos

Description	Sequence
siDNA-PKcs #1	GCGUUGGAGUGCUACAACA[dT][dT]
siDNA-PKcs #2	CAAGCGACUUUAUAGCCUU[dT][dT]
siDNA-PKcs #3	GACCCUGUUGACAGUACUU[dT][dT]
siATM #1	GCUGUUACCUGUUUGAAAA[dT][dT]
siATM #2	CACCUGUUUGUUAGUUUAU[dT][dT]
siATM #3	CAGCUGUCAUCAUAUAAGA[dT][dT]
siATR #1	GAGCCGAUUUUUAAGUCAA[dT][dT]
siATR #2	GAUGAGUAUGCAAAAUUUA[dT][dT]
siATR #3	GCCGCUAAUCUUCUAACAU[dT][dT]

DNA Oligos

Description	Sequence
SSA1 gDNA T492E Forward	TCGATGTCGACTCTAACGGTATTTTGAATGTTTCCGCCGTCGAAAAGGGTGAAGGTAAGTCTAACAAG
SSA1 gDNA T492A Forward	TCGATGTCGACTCTAACGGTATTTTGAATGTTTCCGCCGTCGAAAAGGGTGCTGGTAAGTCTAACAAG
SSA1 gDNA Reverse	CAGATCATTAAAAGACATTTTCGTTATTATCAATTGCCGCACCAATTGGCGCATGCCGGTAGAGG
SSA2-KanMx Forward	TTGATTAATTCCAACAGATCAAGCAGATTTTATACAGAAATATTTATACAATGGGTAAGGAAAAGACTCA
KanMx-Ssa2 Reverse	GGAAAGCAAAAGTAAAACTTTTCGGATATTTTACAGGGCGATCGCTAAGCTTAGAAAAACTCATCGAGCA

Antibodies

Antigen	Dilution	Supplier (catalog #)
pHsp70	1:5000	Custom (Moss 2019)[12]
GAPDH	1:3000	Proteintech (60004-1-Ig)
γH2AX	1:1000	Millipore Sigma (05-636)
Hsp70	1:1000	Santa Cruz Biotechnology (sc-66048)
pDNA-PKcs (S2056)	1:1000	Abcam (ab18192)
pChk2 (T68)	1:1000	Cell Signaling Technology (2197T)
Hsp90	1:1000	Cell Signaling Technology (4874S)
pChk2 (S516)	1:1000	Cell Signaling Technology (2669T)
pATM (S1981)	1:1000	Cell Signaling Technology (4526S)
Tubulin	1:3000	Proteintech (66031-1-Ig)

Thymidine Kinase	1:1000	Cell Signaling Technology (28755S)
pCdk1 (Y15)	1:1000	Cell Signaling Technology (4539S)
Cyclin B	1:500	Santa Cruz Biotechnology (sc-245)
pHistone H3 (S10)	1:1000	Cell Signaling Technology (53348S)
Cyclin E	1:1000	Santa Cruz Biotechnology (sc-247)
CDT1	1:1000	Cell Signaling Technology (8064S)
Lamin B1	1:1000	Proteintech (12987-1-AP)
Cyclin A	1:1000	Santa Cruz Biotechnology (sc-271682)
Polβ	1:1000	Proteintech (18003-1-AP)
APE1	1:1000	Proteintech (10203-1-AP)
ATM	1:1000	Cell Signaling Technology (2873S)
ATR	1:1000	Cell Signaling Technology (2790S)

Yeast Strains

Description	ID
Parental W303α	Y017
Ssa1(WT)-NAT #1	Y019
Ssa1(WT)-NAT #2	Y034
Ssa1(T492A)-NAT #1	Y040
Ssa1(T492A)-NAT #2	Y041
Ssa1(T492E)-NAT #1	Y038
Ssa1(T492E)-NAT #2	Y039
Ssa1(WT)-NAT;*ssa2*Δ #1	Y023
Ssa1(WT)-NAT;*ssa2*Δ #2	Y037
Ssa1(T492A)-NAT;*ssa2*Δ #1	Y051
Ssa1(T492A)-NAT;*ssa2*Δ #2	Y046
Ssa1(T492E)-NAT;*ssa2*Δ #1	Y044
Ssa1(T492E)-NAT;*ssa2*Δ #2	Y057

Software

Software	Source	URL
Prism Version 10.4.2	Graphpad	https://www.graphpad.com/scientific-software/prism/
ImageLab 6.0.1	Biorad	https://www.bio-rad.com/en-us/product/image-lab-software?ID=KRE6P5E8Z
FlowJo™ 10.10.0	BD Life Sciences	https://flowjo.com/flowjo/download
UCSF Chimera X v1.3	Pettersen et al.[49]	https://www.rbvi.ucsf.edu/chimera

METHODS

Cell Culture

HEK293T and HeLa lines were obtained from ATCC. All cell lines were regularly tested for mycoplasma contamination. Cells were maintained in Dulbecco's modified Eagle's medium (DMEM, Gibco) supplemented with 10% fetal bovine serum (FBS, VWR) in a humidified incubator at 37°C, 5% CO_2. Cells were treated with 10 mM methyl methanesulfonate (MMS) (Fisher AC156890050) for 5 h unless otherwise indicated. Cells were treated with methoxyamine hydrochloride (Sigma Aldrich 226904), APE1 compound III (EMD Millipore 262017), bleomycin (sulfate) (Thomas Scientific C830H18), camptothecin (Selleck S1288), hydroxyurea (Sigma-Aldrich H8627), sodium arsenite (Fisher Scientific S88733), KU-60019 (MedChem Express HY-12061), AZD1390 (MedChem Express 2089288-03-7), CCT241533 (MedChem Express HY-14715B), PF-670462 (Sigma-Aldrich SML0795), thymidine (Fisher 501882638), Ro-3306 (MedChem Express HY-12529), and AZD7648 (MedChem Express 2230820-11-6) as described in the figure legends.

siRNA and Plasmid Transfection of Mammalian Cells

Cells were transfected with high quality maxiprepped plasmid DNA (Sigma Genelute HP kit), custom synthesized siRNA duplexes (Sigma-Aldrich VC30002), or Mission® siRNA Universal Negative Control #1 (Sigma Aldrich SIC001) using the jetPRIME transfection system (VWR 89129-926). For plasmid transfection, cells were grown to 70% confluence and transfected overnight with total µg of DNA added as recommended by supplier for the culture vessel. For siRNA transfection, knockdowns were performed per manufacturer suggestions in HeLa cells. Cells were transfected for 24 h after which the media was replaced with fresh media. Cells were allowed to grow for an additional 48 h before any additional treatment and harvesting.

Whole Cell Lysate Preparation and Western Blotting

Once experimental manipulations were complete, media was aspirated and cells were washed 3X with ice cold 1X TBS on ice. Cells were gently scraped into 1 mL ice cold 1X TBS and transferred to 1.5 mL microcentrifuge tubes. Cells were pelleted at 3000xg for 5 min at 4°C, and the supernatant was aspirated. Pellets were stored at -80°C until lysis.

1x RIPA lysis buffer (Cell Signaling Technology 9806S) supplemented with 1x Roche cOmplete protease inhibitor cocktail (Roche 11697498001), 1x Roche PhosStop (Roche 04906837001), and 1mM PMSF was added to the frozen pellets which were then agitated for 30 min at 4 °C then centrifuged at 16,000 xg for 15 min at 4 °C. Cleared lysates were transferred to a new tube, and protein concentrations were quantified using the Pierce BCA Assay Kit (Thermo Scientific 23227). 30-100 µg total protein was denatured in 1x SDS sample buffer with 10mM dithiothreitol (DTT) for 8 min at 95 °C. Lysates were loaded onto polyacrylamide gels (8, 10% or Bio-Rad Mini-PROTEAN TGX Precast Protein Gels, 4-20%) (BioRad) and separated by SDS-PAGE. Proteins were transferred to methanol-activated 0.2 µm pore PVDF membranes overnight at 4°C in 1X CAPS, 10% methanol. Membranes were blocked in either 5% bovine serum albumin (BSA) (VWR) for phopsho-specific antibodies, or 5% non-fat dry milk (BioRad) in TBS-T (0.1% Tween-20 in TBS) for 1 h at RT. Primary antibodies were diluted in 5% BSA, 0.02% NaN_3 in TBS-T. Membranes were incubated with primary antibody solutions overnight at 4°C. Membranes were washed 3X in TBS-T for 10 min each wash, then incubated with 1:5000 secondary antibody in blocking buffer for 1 h at RT. Membranes were washed 3X in TBS-T for 10 min each wash, then developed for 1 min in Amersham ECL Western Blotting Detection Reagent (Cytiva RPN2209) or Immobilon Crescendo (Millipore WBLUR0500) and imaged on a ChemiDoc Imaging System (BioRad).

Nuclear and Cytoplasmic Extraction

Nuclear and cytoplasmic extraction was performed at 4 °C using the NE-PER Nuclear and Cytoplasmic Reagents (Fisher Scientific PI78835, Thermo Scientific 78833) following the manufacturer's protocol. Protein quantification and Western blotting was performed as described above.

449
450 Protein Purification
451 Hsc70 and point mutants were purified as described previously[50]. In brief, plasmids containing
452 His-tag proteins were transformed into Rosetta(DE3) *E. coli*. Bacteria were grown in 2 L Terrific
453 Broth (TB) to OD_{600}=0.6. Bacterial cultures were cooled to 20 °C, and protein expression was
454 induced with 200μM IPTG at 20 °C overnight. The cells were harvested by centrifugation (7500
455 r.p.m. 10 min, JLA 8.1 rotor) and then resuspended in 20 mL His-Binding Buffer (50 mM Tris, 10
456 mM imidazole, 500 mM NaCl, pH 8) + 2 tablets EDTA-free Roche cOmplete Protease Inhibitor
457 per liter culture using a Dounce homogenizer. Cells were then lysed by sonication at Amp 35%
458 for 5 min, 30 sec on, 30 sec off, on ice at 4 °C. Lysate was separated by centrifugation (18000
459 r.p.m. 30 min, JA-20 Beckman rotor) and incubated with 10 mL/L pre-equilibrated Ni-NTA resin
460 (EMD Millipore 70666-5)/liter of culture at 4 °C for 1 h. Bound protein was first washed with 200
461 mL His-binding buffer, then 100 mL His-Washing buffer (50 mM Tris, 30 mM imidazole, 300 mM
462 NaCl, pH 8) , and then eluted with His-Elution buffer (50 mM Tris, 300 mM imidazole, 300 mM
463 NaCl, pH 8). This His-tag was then removed by the spiking in 5 mM β-mercaptoethanol and 600
464 μg TEV protease to the sample and dialyzing overnight into Buffer A (25 mM HEPES, 5 mM $MgCl_2$,
465 10 mM KCl, pH 7.5) in 10 KDa MWCO snakeskin dialysis tubing (Thermo Fisher 68100). The
466 protein was further purified by an ATP-agarose column using previously established protocols[50].
467 Purified DnaJA2 and tau were acquired from J.E.G.
468
469 ATPase Assays with Malachite Green
470 The ATPase activity of Hsc70 and Hsc70(T495E) was performed with malachite green (MG)
471 (Sigma Aldrich) as described previously[51]. Briefly, in a clear 96-well plate, Hsc70 or Hsc70(T495E)
472 were incubated with increasing concentrations of human DnaJA2 (DJA2) in 25 μL total volume.
473 Reactions were also performed with DnaJA2 in the absence of Hsc70 for background subtraction.
474 The assay buffer was 100 mM Tris at pH 7.4, 20 mM KCl, 6 mM $MgCl_2$, and 0.01% Triton. The
475 reaction was initiated by the addition of ATP at a final concentration of 1 mM and incubated at
476 37 °C for 1 h. After incubation, 80 μL of MG reagent was added, followed by 10 μL of saturated
477 sodium citrate to quench the reaction. Absorbance was measured at 620 nm on a SpectraMax
478 M5 plate reader (Molecular Devices). ATP hydrolysis rates were calculated by comparison to a
479 phosphate standard. Displayed curves are a combination of 6 replicates.
480
481 Fluorescence Polarization (FP) of ATP-FAM
482 Nucleotide of Hsc70 and Hsc70(T495E) was assessed with a fluorescence polarization (FP)
483 assay using labeled ATP. First, apo-Hsc70 was generated by subsequent 6-12h dialyses in the
484 following buffers: buffer 1 (25 mM HEPES, 100 mM NaCl, 5 mM EDTA (pH 7.5)), buffer 2 (25 mM
485 HEPES, 100 mM NaCl, 1 mM EDTA (pH 7.5)), buffer 3 (25 mM HEPES, 5 mM $MgCl_2$, 10 mM KCl
486 (pH 7.5)). Following this, 40 kDa MWCO Zeba Buffer Exchange columns (Thermo Fisher A57760)
487 were used to exchange the buffer to FP assay buffer 100 mM Tris, 20 mM KCl, 6 mM $MgCl_2$, pH
488 7.4) before protein quantification. The assay was performed in 384-well black round-bottom low-
489 volume plates (Corning 4511). 40 nM ATP-FAM (Jena Bioscience nu-805-5fm) was added to
490 each well for a final concentration of 20 nM in 20 μL. Hsc70 and Hsc70(T495E) were added for a
491 starting concentration of 20 μM in 20 μL, and then serially diluted with FP assay buffer (2-fold 13
492 times into the ATP-FAM. Plates were covered and incubated for 30 min at room temperature.
493 Fluorescence polarization was read on a SpectraMax M5 plate reader (excitation, 485 nm;
494 emission, 535 nm)
495
496 Partial Proteolysis
497 The partial proteolysis protocol to identify Hsp70 conformations was modified from previous
498 work[17]. Hsc70 and Hsc70(T495E) was buffer exchanged to proteolysis buffer (40 mM HEPES,

20 mM NaCl, 8 mM $MgCl_2$, 20 mM KCl, 0.3 mM EDTA, pH 8) using Zeba 40 kDa MWCO buffer exchange columns and diluted to 3 μM in this buffer. ATP or ADP was added to 1 mM and incubated for 30 min at room temperature. 1.5 μM trypsin (Sigma EC 3.4.21.4) was added for 2 h at room temperature. The reaction was quenched by boiling in SDS loading buffer (125 mM Tris-HCl pH 6.8, 5% SDS, 10% β-mercaptoethanol, 20% glycerol, 0.025% bromophenol blue), run on a precast SDS-PAGE gel (Bio-Rad) and stained by Coomassie.

Hsc70-tau binding ELISA

Hsc70-tau ELISA was modified from a previously published protocol[52]. It was performed in a Fisherbrand, Flat bottom 96-well plates, clear, PS (cat no 12565501). 1μM Hsc70 or Hsc70(T495E) (diluted in dialysis buffer 3 from FP assay) was added to wells along with 1 mM ATP and incubated overnight at 37°C. Protein was discarded from wells followed by 3x 3min washes on rocker with PBS-T, discarding the PBS-T and vigorously blotting the inverted plate on a paper towel between each wash. In triplicate, add 30 uL of tau to each well, spanning a 12-dose 3-fold concentration gradient (from 70 μM). Plates were covered and incubated at room temperature for 3 h. Solutions were removed and wells washed 3x with PBS-T as described above. 100 μL of blocking solution (5% non-fat milk in TBS-T) was added to all wells and incubated at room temperature for 5 min without rocking. Solution was removed without washing. 50 uL of primary antibody was added to all wells (1:2000 mouse anti-tau clone D-8 from SantaCruz Biotechnologies in blocking solution). The plate was incubated for 1 h at room temperature without shaking. Solution was removed and wells washed 3x with PBS-T. 50 μL of secondary antibody (1:2000 goat anti-mouse (Jackson 115-035-146)in blocking solution) was added to the wells. The plate was incubated for 1h at room temperature and then washed 3x with PBS-T. 50 μL of TMB substrate was added to the wells (ThermoFisher 34028) and incubated for 15 min at room temperature in the dark. 50 μL 1M HCl was added and the plate read at 450 nm on SpectraMax M5 plate reader.

Yeast Strain Generation

W303α yeast and W303α yeast with SSA1 NAT were gifted to us by David Morgan. Oligos for yeast point mutations were generated by PCR amplification of NAT-SSA1with the relevant codon substituted in the primer sequence. Oligos for SSA2 interruption were generated by PCR amplification of KanMX from pYM13 with flanking sequences to SSA2. gDNA was extracted from yeast by first suspending yeast colonies from a YPAD plate in 100 μL LiOAc/SDS buffer (0.2 M LiOAc, 1% SDS). Cells were incubated at 70 °C for 10 min, and then 300 μL 96-100% ethanol was added. Sample was then mixed by vortexing. Sample was the spun at 15,000 xg for 3 min, supernatant removed, and pellet dissolved in 100 μL nuclease free water. The sample was then spun down at maximum speed for >15 sec, and supernatant was transferred to a new tube. 1 μL of supernatant was used for subsequent PCRs.

For yeast transformations, competent cells were generated by first diluting an overnight culture 1:20 in YPAD and grown on a rotary shaker at 30 °C to mid-log. The yeast were spun at 3000 xg for 1min. While spinning the yeast, 10 mg/mL salmon sperm DNA (Sigma-Aldrich D9156) was boiled for 5 min and then put on ice. The supernatant was removed from the yeast pellet which was then washed 1x in water and re-pelleted. The water was remove and the yeast was resuspended in LiOAc/TE solution (10 mM Tris-HCl pH 8, 1 mM EDTA, 0.1 M lithium acetate (Sigma-Aldrich L4158)). This was then pelleted, the supernatant aspirated, and yeast were resuspended in 200 uL LiOAc/TE solution to generate competent cells. For each transformation, 50uL of these competent cells were mixed with 1μg of DNA along with 10 μL of boiled salmon sperm DNA and 500 μL of PEG/LiOAc/TE solution (10 mM Tris-HCl pH 8, 1 mM EDTA, 0.1 M lithium acetate, 40% PEG 3350). This mix was incubated at 30 °C with shaking at 550 r,p,m, on a ThermoMixer F1.5 (Eppendorf), then spun for 1 min at 3000 xg. The supernatant was removed

and the yeast resuspended in sterile water and plated on YPAD and grown overnight at 30 °C. The following day, these plates were replica plated onto plates with the appropriate selection marker.

Yeast Growth

For all yeast experiments, yeast were first grown overnight in YPAD on a rotary shaker at 30 °C. The following morning, yeast were diluted to OD_{600} =0.3 and grown at 30 °C to midlog (OD_{600} = ~0.6). Strains were then concentrated (by centrifugation at 3000xg) to 2e7 cells/mL in 1.5 mL microcentrifuge tubes.

Growth Curve

The above yeast were diluted 1:30 into a clear flat bottom 96 well plate (Costar 3370) and grown for 25 h with continuous orbital shaking at 30 °C on a Cytation 5 Imaging Reader (BioTek) with OD_{600} collected every 20 min.

Yeast Spot Test

The day prior to the experiment, Nunc Rectangular Dishes (Thermo 267060) were made with either YPAD or YPAD + 0.0095% MMS. The above yeast were serially diluted 10-fold 5 times. 5 µL of the dilutions were spotted on the YPAD or YPAD + MMS plates. Plates were grown for three days at 30 °C and imaged daily on a ChemiDoc Imaging System (BioRad).

Yeast Cell Cycle Analysis

This protocol was modified from previous work[53,54] For cell cycle analysis of yeast at mid-log, we took 500 µL of the 2e7 cell/mL yeast solution, spun it at 14,000 xg for 30 sec, removed the supernatant, washed 1x in water and re-pelleted. The water was then decanted, and the yeast were vortexed to resuspend them in the water remaining in the tube. 95% ethanol prechilled to -20 °C was added to the resuspended yeast which were then vortexed and placed on ice. For MMS treatment, yeast were grown to mid-log as previously described. 0.05% MMS (Fisher Scientific AC156890050) was then added to the yeast for 3 h[13], rotating at 30 °C. Samples were harvested as described for 'no recovery' conditions, and the remaining yeast was transferred to 15 mL centrifuge tubes (Fisher Scientific 12-565-268),spun at 300 xg. The pellet was washed 1x with sterile water, spun down again, and then resuspended in the starting volume of YPAD. The caps were partially unscrewed and the yeast was returned to the rotary at 30 °C with samples harvested as detailed above at the indicated time points. Once all samples were resuspended in ethanol the yeast were stored at -20 °C for at least overnight. The yeast were then resuspended by vortexing and spun at 14000 xg for 1 min. The ethanol was removed, the yeast resuspended in water and then pelleted again. The water was removed and the pellet was resuspended in 1mL sodium citrate buffer (50 mM sodium citrate (C8532), pH to 7.5 with citric acid (BP399)). 8 µL of 10 mg/mL RNAase A (Thermo EN0531) was then added to the samples and incubated for 2 h at 37 °C. Following this, 10 µL of 20 mg/mL Proteinase K (NEB P8107S) was added to the samples and incubated for 1 h at 50 °C. The samples were then incubated at 4 °C overnight. The samples were spun down at 14000 xg for 1 min and the pellets resuspended in 500 µL sodium citrate buffer + 2.5 µM SYTOX Green (Thermo Fisher S7020), or sodium citrate buffer alone for the no-stain control. Samples were placed on ice and sonicated with a probe sonicator (QSonica) at 30% amplitude for 10 sec. The samples were then stored in the dark at 4 °C until flow cytometry analysis.

All yeast flow cytometry experiments were performed on a LSRII SORP (BD Biosciences) using a 488 nm laser, and the software analysis done on FlowJo (10.10.0). Cells were first selected by graphing FSC-A by SSC-A. Singlets were then gated by graphing FSC-A by FSC-H and then analyzed.

Data Reproducibility and Statistical Analysis

All statistics were performed in Prism as described in the relevant figure legends. Figures are either mean + SD, or representative of the number of replicates described in the figure legend.

ACKNOWLEDGEMENTS

We thank Dr. Adriana Steinbach and Dr. Michael Metrick for critical evaluation and discussions of the data. We thank Dr. Henry Ng and Dr. David O. Morgan for yeast strains and technical advice. We thank Dr. Oleta Johnson, Dr. Cory Nadel, and Dr. Emma Carroll from the J.E.G. lab for technical assistance and advice. We acknowledge Vinh Nguyen for his technical support and the PFCC (RRID:*SCR_018206*) for assistance generating Flow Cytometry data. Research reported here was supported in part by the DRC Center Grant NIH P30 DK063720. T.M. acknowledges support from the MPHD T32 training grant. J.E.G. acknowledges support from R01NS059690. S.M. acknowledges financial support from the National Institutes of Health (grant nos. R01GM140440 and R01GM144378), the Pew Charitable Trust (grant no. A129837), a Bowes Biomedical Investigator award, and a gift fund from the Chan-Zuckerberg Biohub.

Author contributions

Conceptualization, T.M., S.M.; Experiment design, T.M., J.E.G., S.M.; Experimentation, T.M., A.W. K.B. M.C..; Formal Analysis, T.M..; Writing, T.M., S.M.; Review & Editing T.M, A.W., J.E.G., S.M.; Funding Acquisition: J.E.G., S.M.

REFERENCES

1. Rosenzweig, R., Nillegoda, N. B., Mayer, M. P. & Bukau, B. The Hsp70 chaperone network. *Nat. Rev. Mol. Cell Biol.* **20**, 665–680 (2019).
2. Kaushik, S. & Cuervo, A. M. The coming of age of chaperone-mediated autophagy. *Nat. Rev. Mol. Cell Biol.* **19**, 365–381 (2018).
3. Dubrez, L., Causse, S., Bonan, N. B., Dumétier, B. & Garrido, C. Heat-shock proteins: chaperoning DNA repair. *Oncogene* **39**, 516–529 (2020).
4. Truman, A. W. *et al.* CDK-Dependent Hsp70 Phosphorylation Controls G1 Cyclin Abundance and Cell-Cycle Progression. *Cell* **151**, 1308–1318 (2012).
5. Chen, Y.-J. *et al.* HSP70 colocalizes with PLK1 at the centrosome and disturbs spindle dynamics in cells arrested in mitosis by arsenic trioxide. *Arch. Toxicol.* **88**, 1711–1723 (2014).
6. Evans, C. G., Wisén, S. & Gestwicki, J. E. Heat Shock Proteins 70 and 90 Inhibit Early Stages of Amyloid β-(1–42) Aggregation in Vitro *. *J. Biol. Chem.* **281**, 33182–33191 (2006).
7. Valle-Medina, A., Calzada-Mendoza, C. C., Ocharan-Hernández, M. E., Jiménez-Zamarripa, C. A. & Juárez-Cedillo, T. Heat shock protein 70 in Alzheimer's disease and other dementias: A possible alternative therapeutic. *J. Alzheimer's Dis. Rep.* **9**, 25424823241307021 (2025).
8. Calderwood, S. K. & Murshid, A. Molecular Chaperone Accumulation in Cancer and Decrease in Alzheimer's Disease: The Potential Roles of HSF1. *Front. Neurosci.* **11**, 192 (2017).
9. Beltrao, P. *et al.* Systematic Functional Prioritization of Protein Posttranslational Modifications. *Cell* **150**, 413–425 (2012).
10. Preissler, S. *et al.* AMPylation matches BiP activity to client protein load in the endoplasmic reticulum. *eLife* **4**, e12621 (2015).
11. Preissler, S. *et al.* AMPylation targets the rate-limiting step of BiP's ATPase cycle for its functional inactivation. *eLife* **6**, e29428 (2017).
12. Moss, S. M. *et al.* A Legionella pneumophila Kinase Phosphorylates the Hsp70 Chaperone Family to Inhibit Eukaryotic Protein Synthesis. *Cell Host Microbe* **25**, 454-462.e6 (2019).
13. Albuquerque, C. P. *et al.* A Multidimensional Chromatography Technology for In-depth Phosphoproteome Analysis. *Mol. Cell. Proteom.* **7**, 1389–1396 (2008).
14. Holt, L. J. *et al.* Global Analysis of Cdk1 Substrate Phosphorylation Sites Provides Insights into Evolution. *Science* **325**, 1682–1686 (2009).
15. Russell, R., Karzai, A. W., Mehl, A. F. & McMacken, R. DnaJ Dramatically Stimulates ATP Hydrolysis by DnaK: Insight into Targeting of Hsp70 Proteins to Polypeptide Substrates †. *Biochemistry* **38**, 4165–4176 (1999).
16. Preissler, S., Rato, C., Perera, L. A., Saudek, V. & Ron, D. FICD acts bifunctionally to AMPylate and de-AMPylate the endoplasmic reticulum chaperone BiP. *Nat. Struct. Mol. Biol.* **24**, 23–29 (2017).
17. Rinaldi, S. *et al.* A Local Allosteric Network in Heat Shock Protein 70 (Hsp70) Links Inhibitor Binding to Enzyme Activity and Distal Protein–Protein Interactions. *ACS Chem. Biol.* **13**, 3142–3152 (2018).
18. Buchberger, A. *et al.* Nucleotide-induced Conformational Changes in the ATPase and Substrate Binding Domains of the DnaK Chaperone Provide Evidence for Interdomain Communication (*). *J. Biol. Chem.* **270**, 16903–16910 (1995).
19. Kundel, F. *et al.* Hsp70 Inhibits the Nucleation and Elongation of Tau and Sequesters Tau Aggregates with High Affinity. *ACS Chem. Biol.* **13**, 636–646 (2018).
20. Lee, P.-C. & Machner, M. P. The Legionella Effector Kinase LegK7 Hijacks the Host Hippo Pathway to Promote Infection. *Cell Host Microbe* **24**, 429-438.e6 (2018).
21. Thomas, E. N., Kim, K. Q., McHugh, E. P., Marcinkiewicz, T. & Zaher, H. S. Alkylative damage of mRNA leads to ribosome stalling and rescue by trans translation in bacteria. *eLife* **9**, e61984 (2020).
22. Beard, W. A., Horton, J. K., Prasad, R. & Wilson, S. H. Eukaryotic Base Excision Repair: New Approaches Shine Light on Mechanism. *Annu. Rev. Biochem.* **88**, 137–162 (2019).

23. Sedgwick, B. Repairing DNA-methylation damage. *Nat. Rev. Mol. Cell Biol.* **5**, 148–157 (2004).
24. Wyatt, M. D. & Pittman, D. L. Methylating Agents and DNA Repair Responses: Methylated Bases and Sources of Strand Breaks. *Chem. Res. Toxicol.* **19**, 1580–1594 (2006).
25. Fu, D., Calvo, J. A. & Samson, L. D. Balancing repair and tolerance of DNA damage caused by alkylating agents. *Nat. Rev. Cancer* **12**, 104–120 (2012).
26. Srivastava, D. K. *et al.* Mammalian Abasic Site Base Excision Repair IDENTIFICATION OF THE REACTION SEQUENCE AND RATE-DETERMINING STEPS*. *J. Biol. Chem.* **273**, 21203–21209 (1998).
27. Horton, J. K., Prasad, R., Hou, E. & Wilson, S. H. Protection against Methylation-induced Cytotoxicity by DNA Polymerase β-Dependent Long Patch Base Excision Repair*. *J. Biol. Chem.* **275**, 2211–2218 (2000).
28. Bau, D.-T. *et al.* Oxidative DNA adducts and DNA-protein cross-links are the major DNA lesions induced by arsenite. *Environ. Heal. Perspect.* **110**, 753–756 (2002).
29. Ebert, F. *et al.* Arsenicals affect base excision repair by several mechanisms. *Mutat. Res.Fundam. Mol. Mech. Mutagen.* **715**, 32–41 (2011).
30. Sykora, P. & Snow, E. T. Modulation of DNA polymerase beta-dependent base excision repair in cultured human cells after low dose exposure to arsenite. *Toxicol. Appl. Pharmacol.* **228**, 385–394 (2008).
31. Chou, W.-C., Hu, L.-Y., Hsiung, C.-N. & Shen, C.-Y. Initiation of the ATM-Chk2 DNA damage response through the base excision repair pathway. *Carcinogenesis* **36**, 832–840 (2015).
32. Geng, A. *et al.* SIRT2 promotes base excision repair by transcriptionally activating OGG1 in an ATM/ATR-dependent manner. *Nucleic Acids Res.* **52**, 5107–5120 (2024).
33. Choi, S., Gamper, A. M., White, J. S. & Bakkenist, C. J. Inhibition of ATM kinase activity does not phenocopy ATM protein disruption. *Cell Cycle* **9**, 4052–4057 (2010).
34. Menolfi, D. & Zha, S. ATM, ATR and DNA-PKcs kinases—the lessons from the mouse models: inhibition ≠ deletion. *Cell Biosci.* **10**, 8 (2020).
35. Zannini, L., Delia, D. & Buscemi, G. CHK2 kinase in the DNA damage response and beyond. *J. Mol. Cell Biol.* **6**, 442–457 (2014).
36. Tuppi, M. *et al.* Oocyte DNA damage quality control requires consecutive interplay of CHK2 and CK1 to activate p63. *Nat. Struct. Mol. Biol.* **25**, 261–269 (2018).
37. Canman, C. E. *et al.* Activation of the ATM Kinase by Ionizing Radiation and Phosphorylation of p53. *Science* **281**, 1677–1679 (1998).
38. Nikolova, T., Ensminger, M., Löbrich, M. & Kaina, B. Homologous recombination protects mammalian cells from replication-associated DNA double-strand breaks arising in response to methyl methanesulfonate. *DNA Repair* **9**, 1050–1063 (2010).
39. Werner-Washburne, M., Stone, D. E. & Craig, E. A. Complex Interactions Among Members of an Essential Subfamily of hsp70 Genes in Saccharomyces Cerevisiae. *Mol. Cell. Biol.* **7**, 2568–2577 (1987).
40. Craig, E. A. & Jacobsen, K. Mutations of the heat inducible 70 kilodalton genes of yeast confer temperature sensitive growth. *Cell* **38**, 841–849 (1984).
41. Caldecott, K. W. Mammalian DNA base excision repair: Dancing in the moonlight. *DNA Repair* **93**, 102921 (2020).
42. Polyzos, A. A. *et al.* Base excision repair and double strand break repair cooperate to modulate the formation of unrepaired double strand breaks in mouse brain. *Nat. Commun.* **15**, 7726 (2024).
43. Blackford, A. N. & Stucki, M. How Cells Respond to DNA Breaks in Mitosis. *Trends Biochem. Sci.* **45**, 321–331 (2020).
44. Heijink, A. M., Krajewska, M. & Vugt, M. A. T. M. van. The DNA damage response during mitosis. *Mutat. Res.Fundam. Mol. Mech. Mutagen.* **750**, 45–55 (2013).

45. Pramanik, S., Chen, Y. & Bhakat, K. K. Base Excision Repair in Mitotic Cells and the Role of Apurinic/Apyrimidinic Endonuclease 1 (APE1) in Post-Mitotic Transcriptional Reactivation of Genes. *Int. J. Mol. Sci.* **25**, 12735 (2024).
46. Fontaine, S. N. *et al.* Isoform-selective Genetic Inhibition of Constitutive Cytosolic Hsp70 Activity Promotes Client Tau Degradation Using an Altered Co-chaperone Complement*. *J. Biol. Chem.* **290**, 13115–13127 (2015).
47. Muller, P. *et al.* C-terminal phosphorylation of Hsp70 and Hsp90 regulates alternate binding to co-chaperones CHIP and HOP to determine cellular protein folding/degradation balances. *Oncogene* **32**, 3101–3110 (2013).
48. Nitika & Truman, A. W. Cracking the Chaperone Code: Cellular Roles for Hsp70 Phosphorylation. *Trends Biochem. Sci.* **42**, 932–935 (2017).
49. Pettersen, E. F. *et al.* UCSF Chimera—A visualization system for exploratory research and analysis. *J. Comput. Chem.* **25**, 1605–1612 (2004).
50. Chang, L., Thompson, A. D., Ung, P., Carlson, H. A. & Gestwicki, J. E. Mutagenesis Reveals the Complex Relationships between ATPase Rate and the Chaperone Activities of Escherichia coli Heat Shock Protein 70 (Hsp70/DnaK)*. *J. Biol. Chem.* **285**, 21282–21291 (2010).
51. Chang, L. *et al.* High-throughput screen for small molecules that modulate the ATPase activity of the molecular chaperone DnaK. *Anal. Biochem.* **372**, 167–176 (2008).
52. Nadel, C. M. *et al.* Phosphorylation of tau at a single residue inhibits binding to the E3 ubiquitin ligase, CHIP. *Nat. Commun.* **15**, 7972 (2024).
53. Zhang, H. & Siede, W. Cell Cycle Checkpoint Control Protocols. *Methods Mol. Biol. (Clifton, NJ)* **241**, 77–91 (2003).
54. Rosebrock, A. P. Analysis of the Budding Yeast Cell Cycle by Flow Cytometry. *Cold Spring Harb. Protoc.* **2017**, pdb.prot088740 (2017).

Figure Legends

Figure 1. The phosphomimetic Hsc70 T495E mutant adopts an open-like conformation

a) Crystal structure of bovine Hsc70(residues 1-554; PDB: 1YUW). The nucleotide-binding domain (NBD, residues 1-383) is shown in cyan, the interdomain linker (residues 384-394) in green, and the substrate binding domain (SBD, residues 395-506) in magenta. T495 is highlighted in white and marked with an asterisk.
b) J-protein-stimulated ATPase activity of wild-type (WT) and phosphomimetic Hsc70 (T495E) measured by malachite green assay. Data points represent mean + SD of technical triplicates.
c) Fluorescence polarization of ATP-FAM binding to WT and T495E Hsc70. Values were normalized to the minimum and maximum polarization; data points represent mean + SD of technical triplicates.
d) Partial proteolysis of WT and T495E Hsc70 by trypsin in the presence of ATP or ADP. Digestion products were resolved by SDS-PAGE, and band intensities were quantified (bar graph, right). Statistical significance was determined by two-way ANOVA with Šidák's multiple comparisons test (adjusted $p = 0.0002$, $n = 4$ technical replicates).
e) Tau binding to immobilized WT and T495E Hsc70 measured by ELISA. Data points represent mean + SD of technical triplicates.

Figure 2. Base excision repair drives phosphorylation of Hsp70 in human cells

a) Hsp70 phosphorylation by MMS treatment or LegK4 overexpression. HEK293T cells were transiently transfected overnight with LegK4Δ1-58:GFP or treated with 10 mM MMS for 5 h. Phosphorylation at T495 was detected using a phospho-specific antibody to pHsp70 T495; GAPDH was used as a loading control. Data are representative of $n > 3$ independent experiments.
b) Schematic of the base excision repair (BER) pathway, highlighting steps relevant to MMS-induced DNA damage.
c) MPG overexpression increases pHsp70 levels. HEK293T cells were transiently transfected with MPG overnight, treated with MMS, and analyzed by immunoblotting for pHsp70, the loading controls GAPDH and Hsp70, and the DNA damage marker γH2AX. Data are representative of $n = 3$ independent experiments.
d) Inhibition of APE1 reduces MMS-induced pHsc70. Cells were pretreated for 1h with 5μM, 10 μM, or 50 μM APE1 inhibitor (APE1 compound III) before MMS treatment. Hsp70 and pHsp70 were detected by immunoblotting. Data are representative of $n = 3$ independent experiments.
e) Masking of AP sites prevents pHsp70 accumulation. Cells were pretreated with 60 mM methoxyamine (Mx) for 30 min, followed by cotreatment with 30 mM Mx and 10 mM MMS for 5 h. pHsp70, the loading controls GAPDH and Hsp70, and the DNA damage marker γH2AX were detected by immunoblotting. Data are representative of $n = 3$ independent experiments.
f) DNA damage specificity panel for pHsp70 induction. Cells were treated with bleomycin (10 μM, 5 h or 24 h), camptothecin (10 μM, 5 h), hydroxyurea (2 mM, 24 h), MMS (3 mM or 10 mM, 5 h), sodium arsenite (0.5 mM, 5 h), or DMSO vehicle (5 h). Immunoblotting was performed for pHsp70, DDR kinase activation markers (pDNA-PKcs S2056, pChk2

T68, pChk2 S16, pATM S1981), DNA damage marker γH2AX, and loading controls (Hsp70 and Hsp90). Data are representative of n = 3 independent experiments.

Figure 3. DDR kinase activity is upstream of Hsp70 phosphorylation

a. DNA-PKcs knockdown reduces pHsp70 levels. Cells were transiently transfected with three independent siRNAs targeting DNA-PKcs or a scramble control for 72 h, followed by treatment with 10 mM MMS for 5 h. pHsp70 and GAPDH (loading control) were detected by immunoblotting. Data are representative of n = 3 independent experiments.
b. Pharmacological inhibition of ATM decreases pHsp70 induction. Cells were pretreated for 1 h with ATM inhibitors (10 μM KU-60019 or 200nM AZD1390), then treated with 10 mM MMS for 5 h. ATM and DNA-PKcs autoactivation were monitored by immunoblotting pATM (S1981) and pDNA-PKcs (S2056), respectively. Tubulin and total Hsp70 served as loading controls. Data are representative of n = 3 independent experiments.
c. Pharmacological inhibition of ATM, DNA-PKcs, Chk2, and CK1 decrease Hsp70 phosphorylation during MMS treatment. Cells were pretreated for 1h with inhibitors for ATM (200 nM AZD1390), DNA-PKcs (2 μM AZD7648), Chk2 (5 μM CCT241533), CK1(50 μM PF-670462) or with vehicle control (DMSO), then treated with 10mM MMS for 5h. Immunoblotting was performed against pHsp70 and the loading control Hsp70. Data are representative of n = 3 independent experiments.
d. Timecourse of MMS-induced DDR activation and pHsp70 phosphorylation. Cells were treated with 10 mM MMS and harvested hourly. ATM and DNA-PKcs activation were detected by pATM (S1981) and pDNA-PKcs (S2056), respectively. Chk2 activation was monitored by pChk2 (T68) and pChk2 (S516). DNA damage was assessed via γH2AX. Hsp70 and Hsp90 were used as loading controls. Data are representative of n = 3 independent experiments

Figure 4. Mitosis precedes Hsp70 phosphorylation

a. Variable pulse-chase MMS treatment suggests a complex signaling pathway. Cells were treated with 10 mM MMS for 1-5 h, then washed twice with PBS and incubated in MMS-free media for the remainder of the 5 h time period. ATM and DNA-PKcs activation were detected by pATM (S1981) and pDNA-PKcs (S2056), respectively. Chk2 activation was monitored by pChk2 (T68) and pChk2 (S516). DNA damage was assessed by γH2AX. Cell cycle progression was monitored using the S phase markers thymidine kinase (ThyK) and CDT1; mitotic entry marker pCdk1(Y15) (whose dephosphorylation permits M-phase entry), M phase marker phospho-histone H3 (S10) (pH3); and cyclins B and E. GAPDH and Hsp90 served as loading controls. Data are representative of n = 3 independent experiments.
b. Early S-phase synchronization by double thymidine block fails to increase pHsp70 accumulation. Cells were treated with 2.5 mM thymidine for 18 h, released into fresh media for 9 h, then retreated with 2.5 mM thymidine for 17 h. Cells were then washed with PBS and released into fresh media with or without 10 mM MMS. Unsynchronized cells were also treated with 10 mM MMS. Cells were harvested at the indicated time points and immunoblotted for pHsp70, cell cycle markers (pCdk1 Y15, pH3, CDT1, ThyK), and loading controls α-tubulin and Hsp90. Data are representative of n = 2 independent experiments.

c. G2/M stalling by CDK1 inhibition reduces pHsp70 levels. Cells were pretreated with 10 μM CDK1 inhibitor Ro3306 or DMSO for 17.5 h, washed twice with PBS, then treated again with Ro3306 or DMSO in the presence or absence of 10 mM MMS for 5 h. Immunoblotting was performed for pHsp70, cell cycle markers(pCdk1 Y15, pH3, CDT1, cyclin A), DDR markers (pDNA-PKcs S2056, pChk2 T68, γH2AX), and loading controls Hsp70 and Hsp90. Data are representative of n = 3 independent experiments.
d. Subcellular fractionation of pHsp70 during MMS treatment shows nuclear localization. Cells were treated with 10 mM MMS from 1-5 h or left untreated, then fractionated into cytoplasmic and nuclear extracts using the NE-PER kit. Immunoblotting was performed for pHsp70 and total Hsp70 levels; α-tubulin and lamin B1 served as cytoplasmic and nuclear markers, respectively. Data are representative of n = 3 independent experiments.
e. Two-hour MMS pulse chase reveals pHsp70 accumulation post-mitosis. Cells were treated with 10 mM MMS for 2 h, washed twice with PBS, and then incubated in fresh media. Samples were harvested hourly, alongside an untreated control. Immunoblotting was performed for pHsp70, DDR markers (pDNA-PKcs S2056, pChk2 T68, pATM S1981, pChk2 S516, γH2AX), cell cycle markers (cyclin A, pCdk1 Y15, pH3, cyclin B, ThyK), and loading controls Hsp70 and Hsp90. Data are representative of n = 3 independent experiments.

Figure 5. Ssa1 T492 phosphorylation mutations cause cell cycle defects in *S. cerevisiae*

a. Growth curves of *S. cerevisiae* Ssa1 mutants show delayed growth. Indicated yeast mutants were grown to mid-log phase, diluted to the same starting concentration, and monitored overnight at 30 °C in a plate reader. Data represent the average of technical triplicates. Data are representative of n = 3 independent experiments.
b. Half-times ($t_{1/2}$) of both Ssa1 mutants in the *ssa2*Δ background, and of the phosphomimetic mutant in the SSA2 background, are significantly increased. Sigmoidal fits were applied to growth curves to determine $t_{1/2}$ values. The data represent three technical replicates with two biological replicates per strain. Bars represent mean + SD of six replicates (n = 6; 2 biological replicates x 3 technical replicates) Statistical significance was determined by ordinary one-way ANOVA followed by Dunnett's multiple comparison test (** $p = 0.0015$; **** $p < 0.0001$).
c. Cell cycle distribution analysis reveals G1 stalling of Ssa1 phosphomutants. Yeast were grown to mid-log phase, adjusted to the same concentration, and immediately fixed. Cells were stained with Sytox Green and analyzed by flow cytometry to determine DNA content. Histograms display DNA content (X-axis) with 1N corresponding to G1 phase, 2N to G2/M, and intermediate values to S phase. Left: WT SSA2 background; right: Δ*ssa2* background. Data are representative of n = 4 technical replicates with 2 biological replicates per strain.
d. Ssa1 phosphomutants display increased MMS sensitivity in a spot test assay. Yeast were grown to mid-log phase, adjusted to 2e7 cells/mL, serially diluted 1:10, and spotted (5μL) onto YPAD plates with or without 0.0095% MMS. Plates were incubated at 30 °C and imaged after 3 days. Data are representative of n = 3 independent experiments.
e. Ssa1 phosphomutants exhibit perturbed G1/S stalling during MMS recovery. Yeast were grown to mid-log phase, treated with 0.05% MMS for 3 h, washed, and resuspended in fresh media for recovery. Samples were collected at the indicated times points and

analyzed by staining and flow cytometry as described as in (c). Data are representative of n = 2 technical replicates with 2 biological replicates per strain.

Figure 6. Cartoon model of the causes and consequences of Hsp70 phosphorylation

a. Non-helix distorting DNA lesions in M phase lead to Hsp70 phosphorylation through APE1-dependent processing and DDR kinase signaling. Treatment with MMS or sodium arsenite generates lesions that are repaired by BER. In M-phase cells, APE1 processing of these lesions creates DSBs, activating DDR kinases and resulting in phosphorylation of Hsp70 at T495. This phosphorylation persists into G1 and stalls cell cycle progression.
b. Proposed mechanism of G1 arrest by phosphorylated Hsp70 (pHsp70). WT (upper panel): (1,2) Phosphorylation promotes stable interactions between Hsp70, its client, and an accessory protein (e.g. pro-degradation machinery); (3) subsequent dephosphorylation permits client release and degradation, enabling S phase entry. Phosphomimetic (middle panel): (1,2) Phosphomimetic Hsp70 promotes client and accessory protein engagement. Inability to dephosphorylate impairs substrate release, blocking S phase entry. Phosphonull (lower panel):(1) client sampling occurs, but phosphorylation-dependent stabilization is absent; (2) eventual association allows (3) client release and degradation, permitting S phase entry, albeit in a poorly regulated manner.

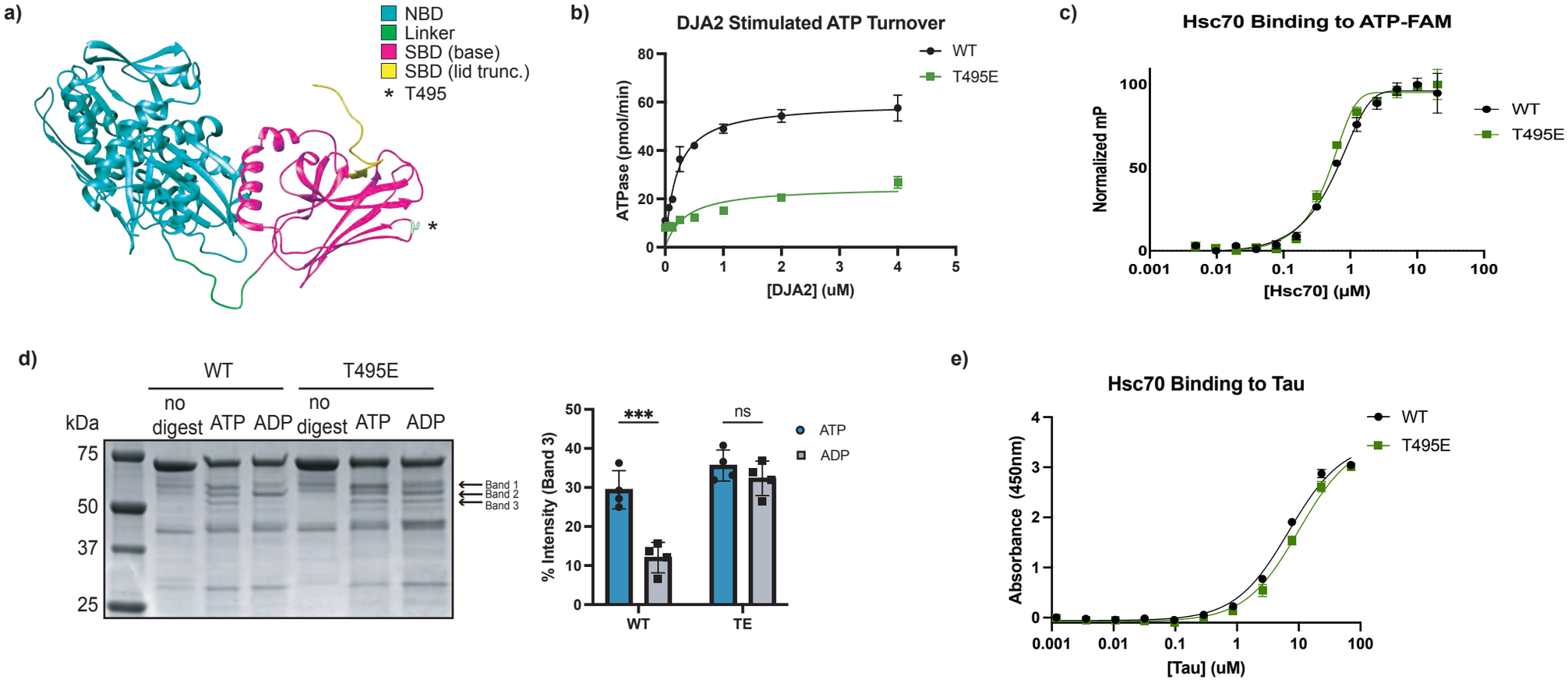
a)
NBD
Linker
SBD (base)
SBD (lid trunc.)
* T495
*
b)
DJA2 Stimulated ATP Turnover
WT
T495E
ATPase (pmol/min)
[DJA2] (uM)
c)
Hsc70 Binding to ATP-FAM
WT
T495E
Normalized mP
[Hsc70] (μM)
d)
WT
T495E
kDa
no digest
ATP
ADP
no digest
ATP
ADP
75
50
37
25
Band 1
Band 2
Band 3
***
ns
ATP
ADP
% Intensity (Band 3)
WT
TE
e)
Hsc70 Binding to Tau
WT
T495E
Absorbance (450nm)
[Tau] (uM)

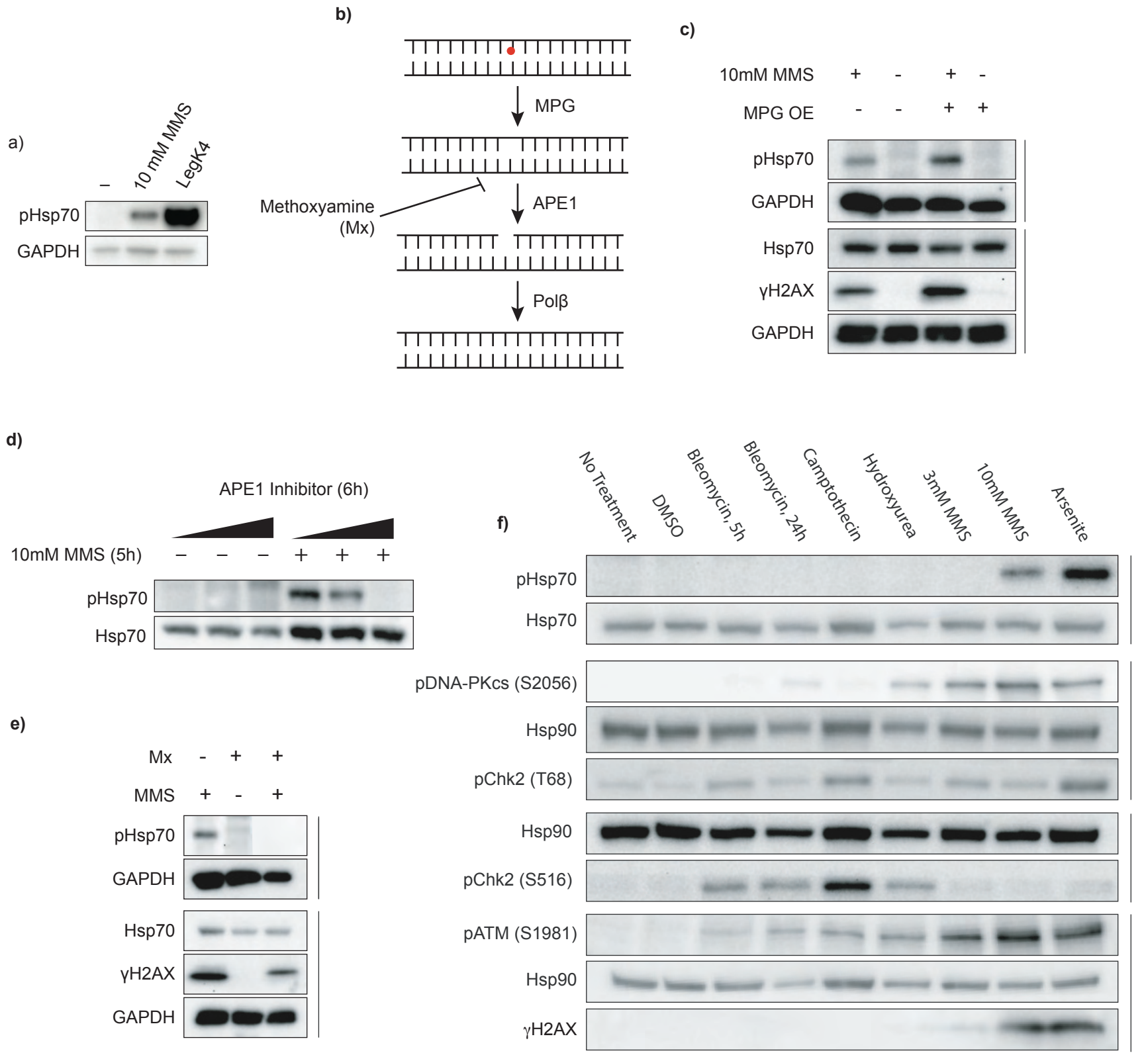
a)
–
10 mM MMS
LegK4
pHsp70
GAPDH
b)
MPG
Methoxyamine
(Mx)
APE1
Polβ
c)
10mM MMS + - + -
MPG OE - - + +
pHsp70
GAPDH
Hsp70
γH2AX
GAPDH
d)
APE1 Inhibitor (6h)
10mM MMS (5h) – – – + + +
pHsp70
Hsp70
e)
Mx - + +
MMS + - +
pHsp70
GAPDH
Hsp70
γH2AX
GAPDH
f)
No Treatment
DMSO
Bleomycin, 5h
Bleomycin, 24h
Camptothecin
Hydroxyurea
3mM MMS
10mM MMS
Arsenite
pHsp70
Hsp70
pDNA-PKcs (S2056)
Hsp90
pChk2 (T68)
Hsp90
pChk2 (S516)
pATM (S1981)
Hsp90
γH2AX

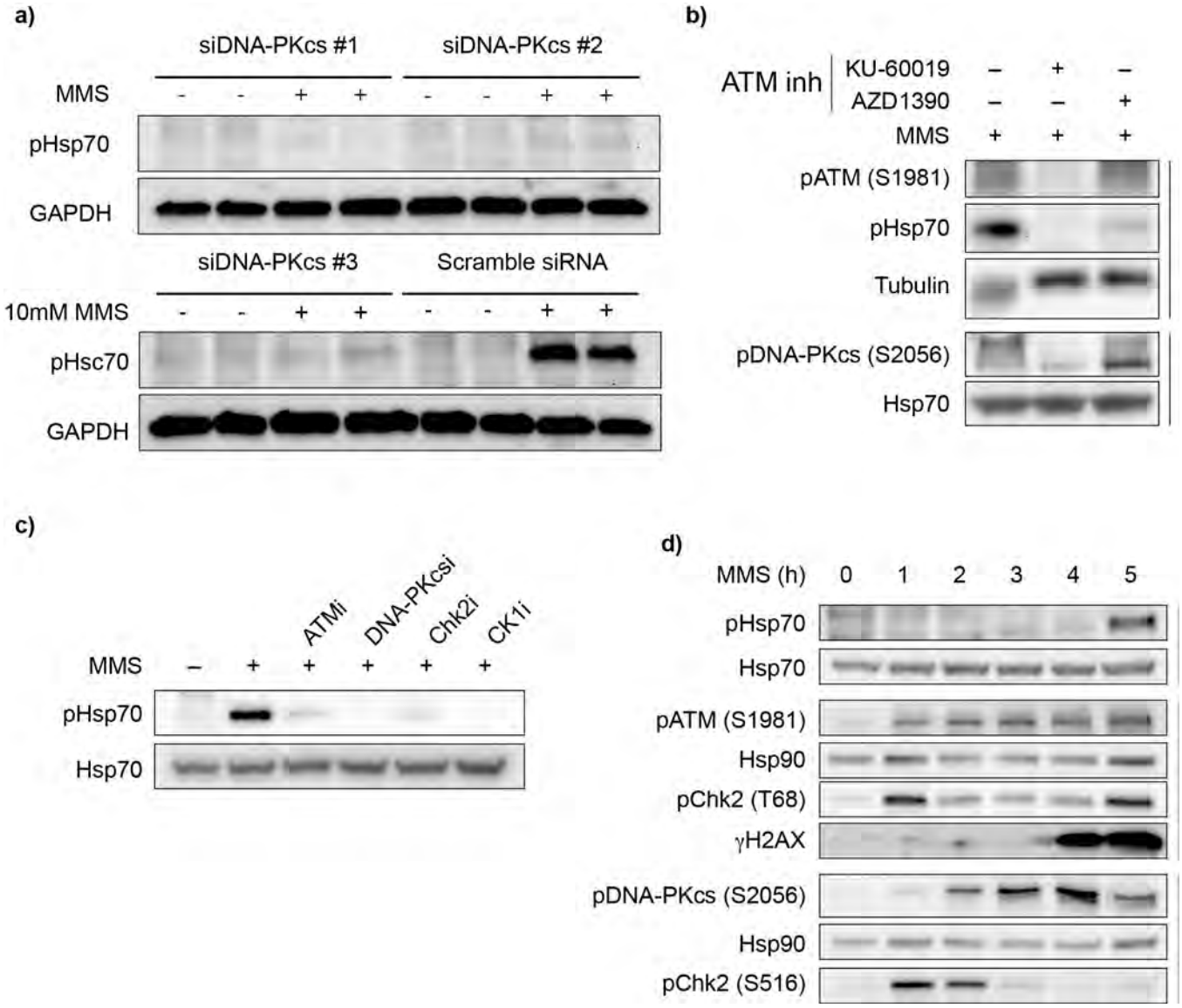
a)
siDNA-PKcs #1
siDNA-PKcs #2
MMS
- - + + - - + +
pHsp70
GAPDH
siDNA-PKcs #3
Scramble siRNA
10mM MMS
- - + + - - + +
pHsc70
GAPDH
b)
ATM inh
KU-60019 – + –
AZD1390 – – +
MMS + + +
pATM (S1981)
pHsp70
Tubulin
pDNA-PKcs (S2056)
Hsp70
c)
ATMi
DNA-PKcsi
Chk2i
CK1i
MMS – + + + + +
pHsp70
Hsp70
d)
MMS (h) 0 1 2 3 4 5
pHsp70
Hsp70
pATM (S1981)
Hsp90
pChk2 (T68)
γH2AX
pDNA-PKcs (S2056)
Hsp90
pChk2 (S516)

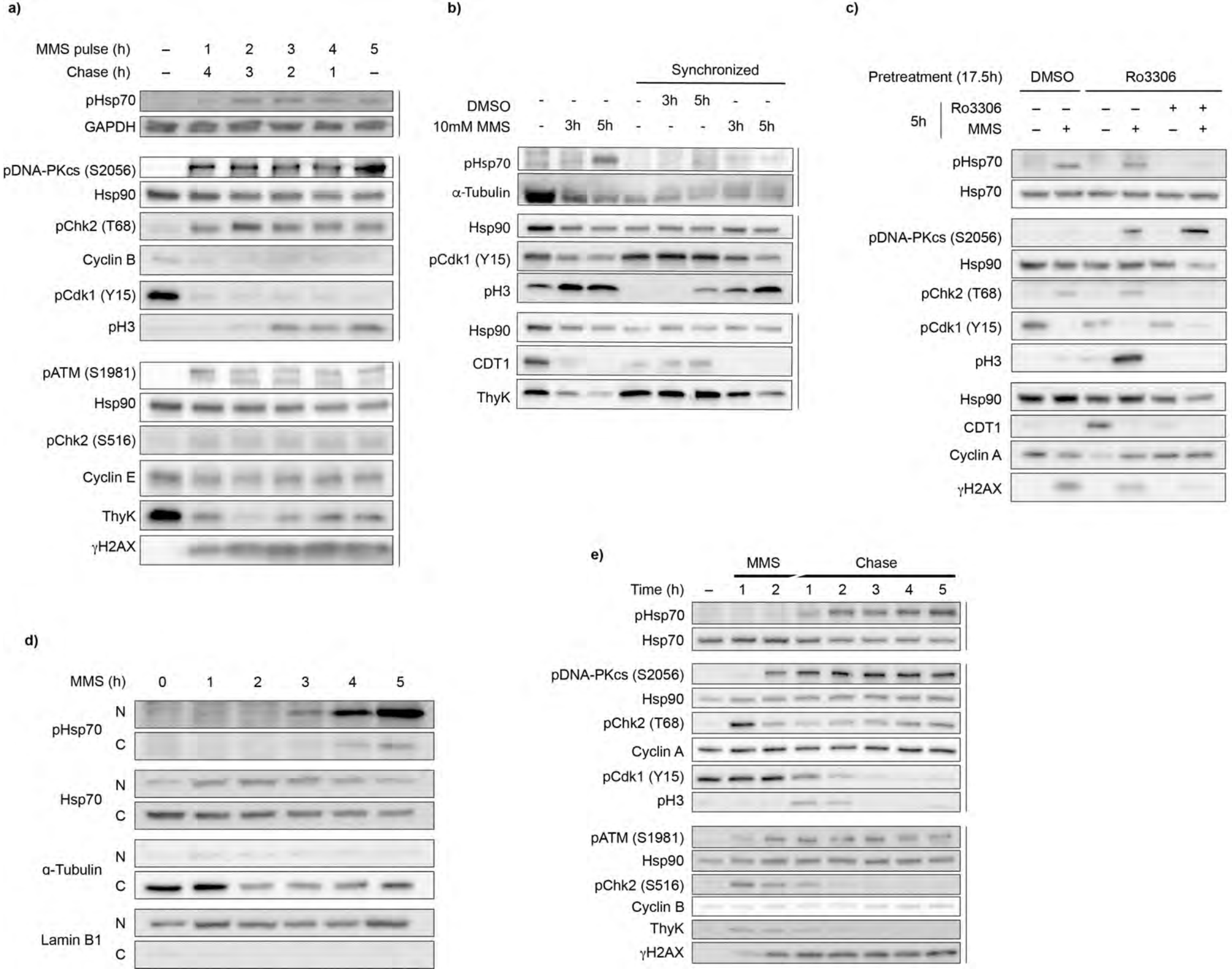
a)
MMS pulse (h) – 1 2 3 4 5
Chase (h) – 4 3 2 1 –
pHsp70
GAPDH
pDNA-PKcs (S2056)
Hsp90
pChk2 (T68)
Cyclin B
pCdk1 (Y15)
pH3
pATM (S1981)
Hsp90
pChk2 (S516)
Cyclin E
ThyK
γH2AX
b)
Synchronized
DMSO - - - - 3h 5h - -
10mM MMS - 3h 5h - - - 3h 5h
pHsp70
α-Tubulin
Hsp90
pCdk1 (Y15)
pH3
Hsp90
CDT1
ThyK
c)
Pretreatment (17.5h) DMSO Ro3306
5h
Ro3306 – – – – + +
MMS – + – + – +
pHsp70
Hsp70
pDNA-PKcs (S2056)
Hsp90
pChk2 (T68)
pCdk1 (Y15)
pH3
Hsp90
CDT1
Cyclin A
γH2AX
d)
MMS (h) 0 1 2 3 4 5
pHsp70 N C
Hsp70 N C
α-Tubulin N C
Lamin B1 N C
e)
MMS Chase
Time (h) – 1 2 1 2 3 4 5
pHsp70
Hsp70
pDNA-PKcs (S2056)
Hsp90
pChk2 (T68)
Cyclin A
pCdk1 (Y15)
pH3
pATM (S1981)
Hsp90
pChk2 (S516)
Cyclin B
ThyK
γH2AX

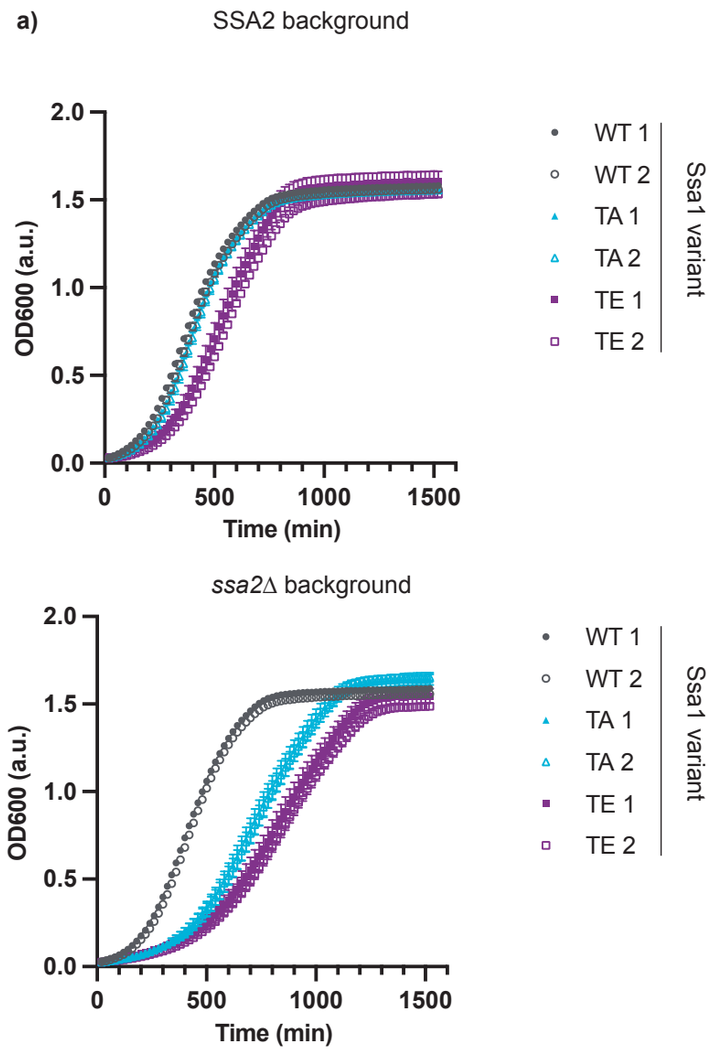
a)
SSA2 background
OD600 (a.u.)
Time (min)
WT 1
WT 2
TA 1
TA 2
TE 1
TE 2
Ssa1 variant
ssa2Δ background

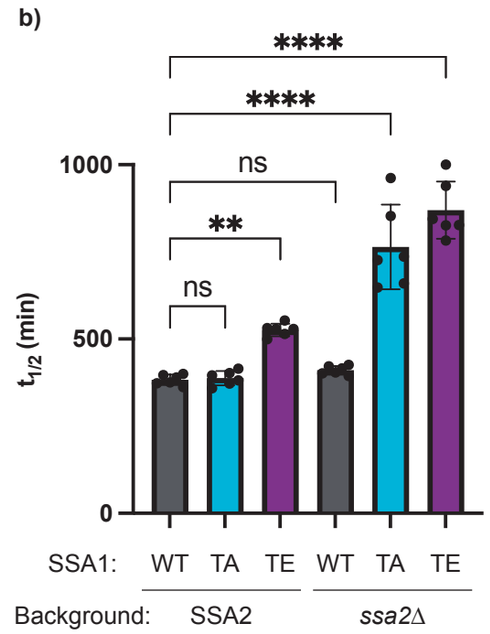
b)
****
****
ns
**
ns
$t_{1/2}$ (min)
SSA1: WT TA TE WT TA TE
Background: SSA2 ssa2Δ

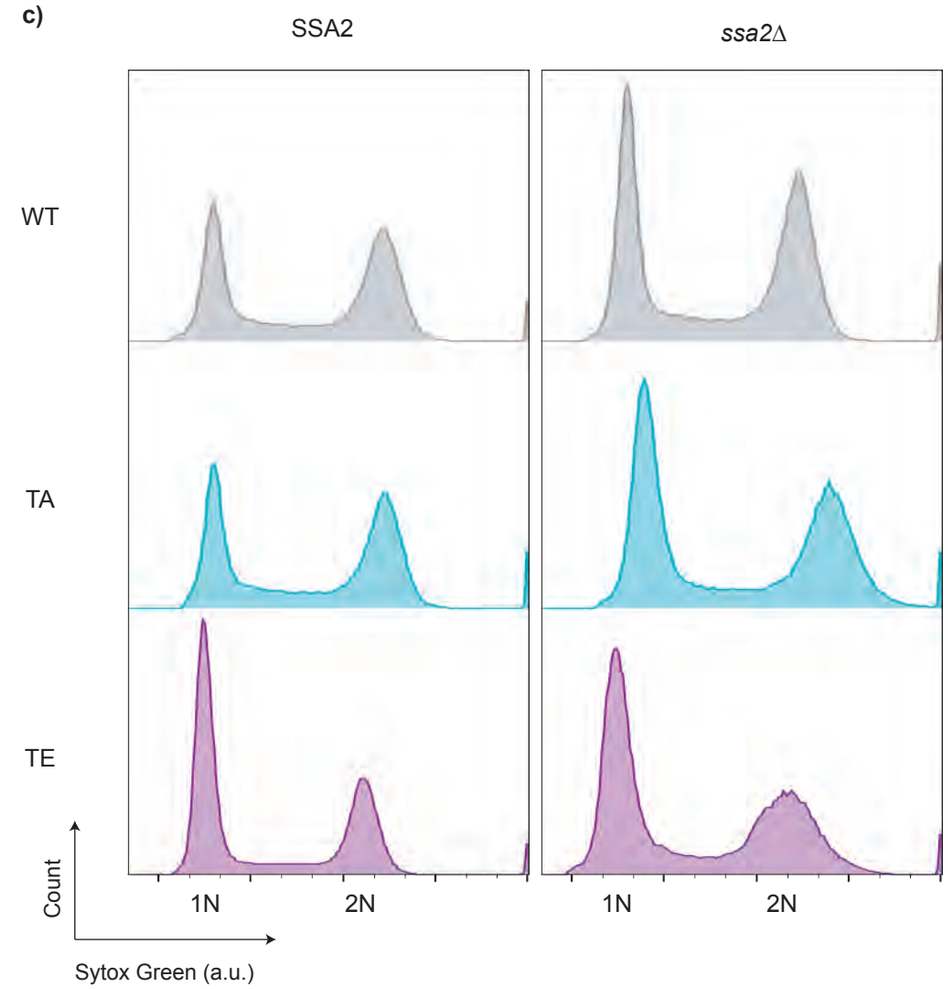
c)
SSA2
ssa2Δ
WT
TA
TE
Count
1N
2N
Sytox Green (a.u.)

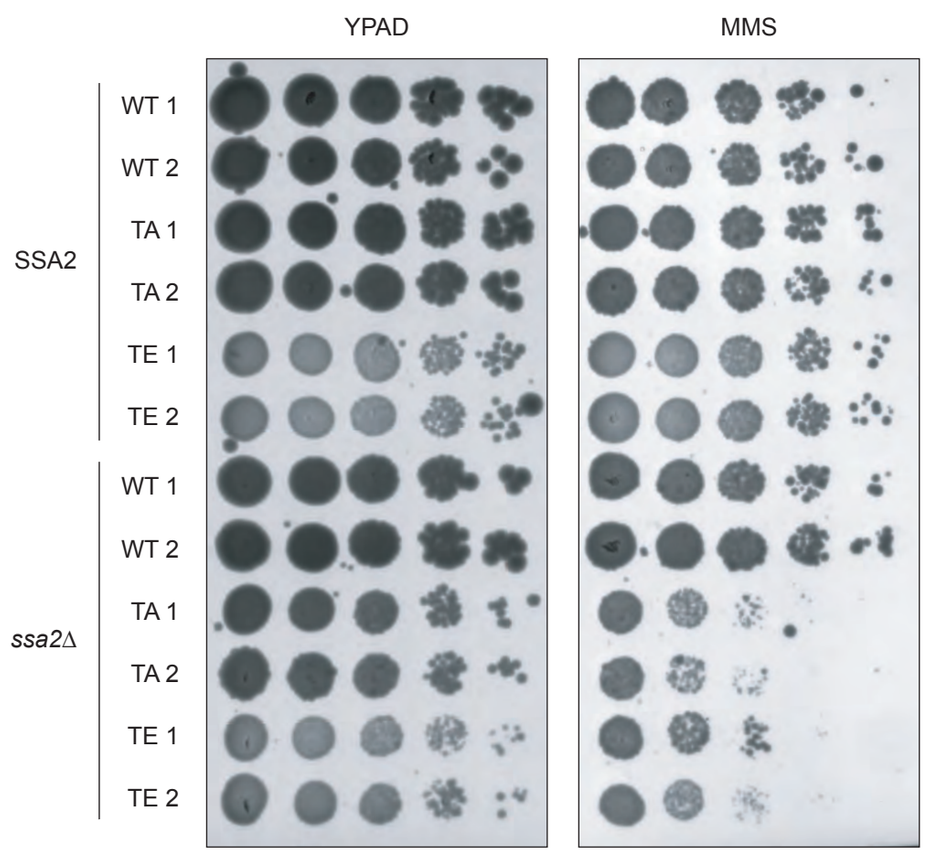
d)
YPAD
MMS
SSA2
ssa2Δ
WT 1
WT 2
TA 1
TA 2
TE 1
TE 2

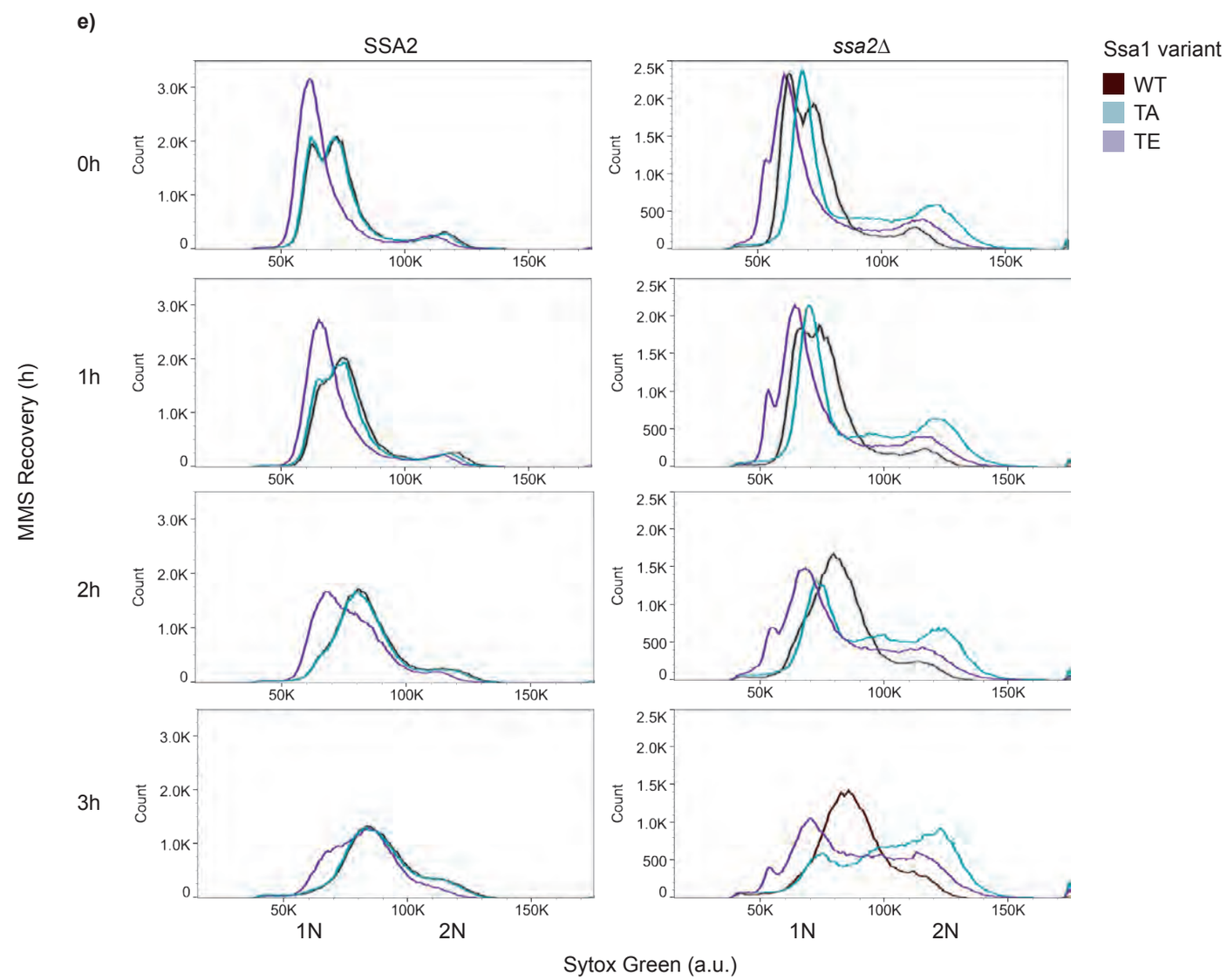
e)
SSA2
ssa2Δ
Ssa1 variant
WT
TA
TE
MMS Recovery (h)
0h
1h
2h
3h
Count
1N
2N
Sytox Green (a.u.)

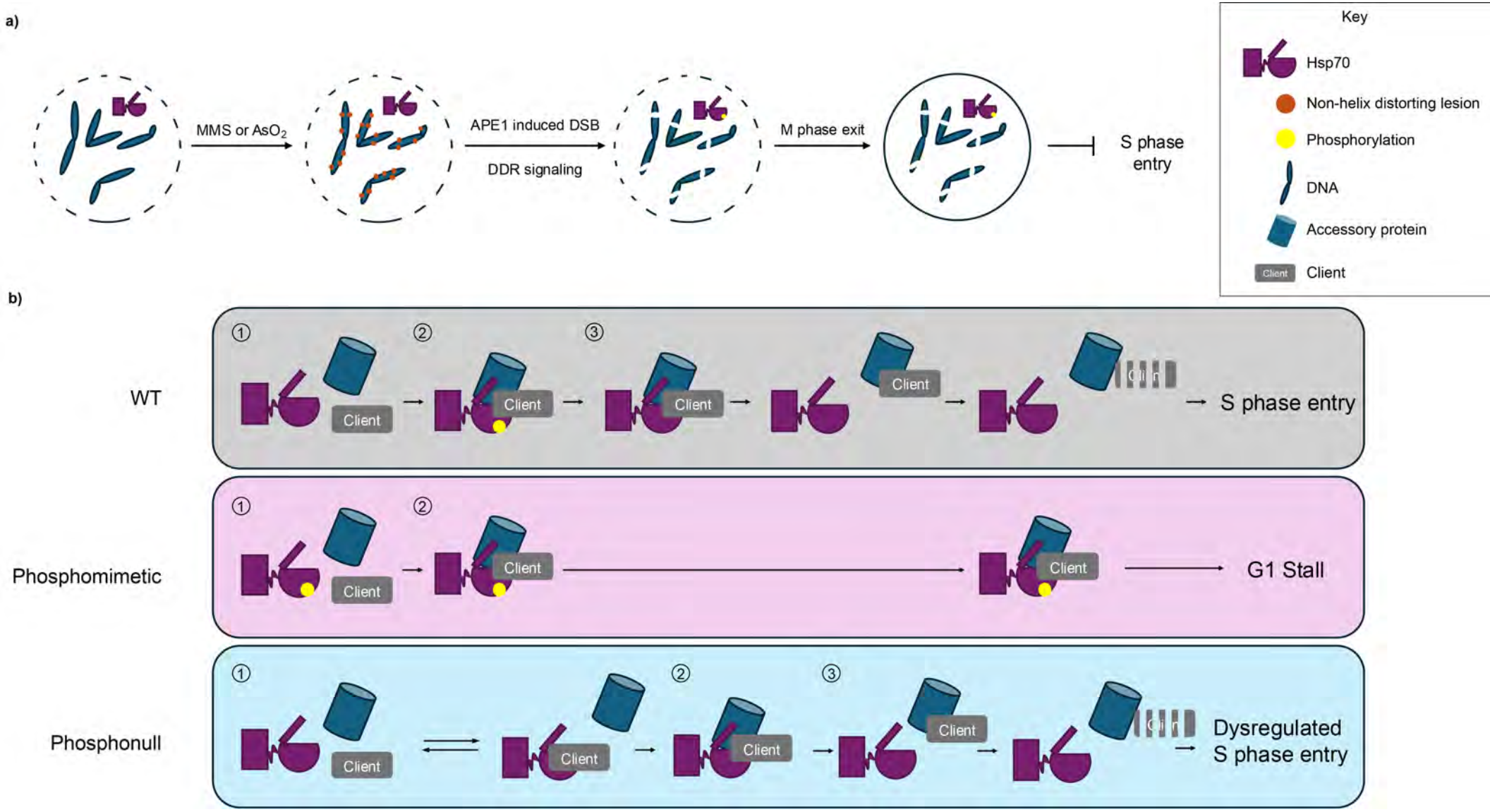
a)
MMS or AsO_2
APE1 induced DSB
DDR signaling
M phase exit
S phase entry
Key
Hsp70
Non-helix distorting lesion
Phosphorylation
DNA
Accessory protein
Client
b)
WT
Client
S phase entry
Phosphomimetic
G1 Stall
Phosphonull
Dysregulated S phase entry